NASA/TM—2013-217810

Unit-Sphere Anisotropic Multiaxial Stochastic-Strength Model Probability Density Distribution for the Orientation of Critical Flaws

Noel N. Nemeth
Glenn Research Center, Cleveland, Ohio

An Erratum was added to this report March 2014.

September 2013

NASA STI Program . . . in Profile

Since its founding, NASA has been dedicated to the advancement of aeronautics and space science. The NASA Scientific and Technical Information (STI) program plays a key part in helping NASA maintain this important role.

The NASA STI Program operates under the auspices of the Agency Chief Information Officer. It collects, organizes, provides for archiving, and disseminates NASA's STI. The NASA STI program provides access to the NASA Aeronautics and Space Database and its public interface, the NASA Technical Reports Server, thus providing one of the largest collections of aeronautical and space science STI in the world. Results are published in both non-NASA channels and by NASA in the NASA STI Report Series, which includes the following report types:

- TECHNICAL PUBLICATION. Reports of completed research or a major significant phase of research that present the results of NASA programs and include extensive data or theoretical analysis. Includes compilations of significant scientific and technical data and information deemed to be of continuing reference value. NASA counterpart of peer-reviewed formal professional papers but has less stringent limitations on manuscript length and extent of graphic presentations.

- TECHNICAL MEMORANDUM. Scientific and technical findings that are preliminary or of specialized interest, e.g., quick release reports, working papers, and bibliographies that contain minimal annotation. Does not contain extensive analysis.

- CONTRACTOR REPORT. Scientific and technical findings by NASA-sponsored contractors and grantees.

- CONFERENCE PUBLICATION. Collected papers from scientific and technical conferences, symposia, seminars, or other meetings sponsored or cosponsored by NASA.

- SPECIAL PUBLICATION. Scientific, technical, or historical information from NASA programs, projects, and missions, often concerned with subjects having substantial public interest.

- TECHNICAL TRANSLATION. English-language translations of foreign scientific and technical material pertinent to NASA's mission.

Specialized services also include creating custom thesauri, building customized databases, organizing and publishing research results.

For more information about the NASA STI program, see the following:

- Access the NASA STI program home page at *http://www.sti.nasa.gov*

- E-mail your question to *help@sti.nasa.gov*

- Fax your question to the NASA STI Information Desk at 443–757–5803

- Phone the NASA STI Information Desk at 443–757–5802

- Write to:
  STI Information Desk
  NASA Center for AeroSpace Information
  7115 Standard Drive
  Hanover, MD 21076–1320

NASA/TM—2013-217810

Unit-Sphere Anisotropic Multiaxial Stochastic-Strength Model Probability Density Distribution for the Orientation of Critical Flaws

Noel N. Nemeth
Glenn Research Center, Cleveland, Ohio

An Erratum was added to this report March 2014.

National Aeronautics and
Space Administration

Glenn Research Center
Cleveland, Ohio 44135

September 2013

Acknowledgments

This work was funded by the NASA Fundamental Aeronautics Program, Supersonics Project.

Erratum

Issued March 2014 for

NASA/TM—2013-217810
Unit-Sphere Anisotropic Multiaxial Stochastic-Strength Model Probability Density Distribution for the Orientation of Critical Flaws
Noel N. Nemeth
September 2013

Page 11: Equation (27) should be

$$\left.\begin{aligned} \zeta(\alpha) &= 0 && 0 \le \alpha < \frac{\pi}{2} - \Lambda_T \\ \zeta(\alpha) &= \left(\sin\left\{ \frac{\pi}{2\Lambda_T}\left[\alpha - \left(\frac{\pi}{2} - \Lambda_T \right) \right] \right\} \right)^{\phi_T} \quad \text{for} && \frac{\pi}{2} - \Lambda_T \le \alpha \le \frac{\pi}{2} \end{aligned}\right\} \tag{27}$$

This work was sponsored by the Fundamental Aeronautics Program at the NASA Glenn Research Center.

Level of Review: This material has been technically reviewed by technical management.

Available from

NASA Center for Aerospace Information
7115 Standard Drive
Hanover, MD 21076–1320

National Technical Information Service
5301 Shawnee Road
Alexandria, VA 22312

Available electronically at http://www.sti.nasa.gov

Unit-Sphere Anisotropic Multiaxial Stochastic-Strength Model Probability Density Distribution for the Orientation of Critical Flaws

Noel N. Nemeth
National Aeronautics and Space Administration
Glenn Research Center
Cleveland, Ohio 44135

Summary

Models that predict the failure probability of monolithic glass and ceramic components under multiaxial loading have been developed by authors such as Batdorf, Evans, and Matsuo. These "unit-sphere" failure models assume that the strength-controlling flaws are randomly oriented, noninteracting planar microcracks of specified geometry but of variable size. This report develops a formulation to describe the probability density distribution of the orientation of critical-strength-controlling flaws that results from an applied load. This distribution is a function of the multiaxial stress state, the shear sensitivity of the flaws, the Weibull modulus, and the strength anisotropy. Examples are provided showing the predicted response on the unit sphere for various stress states for isotropic and transversely isotropic (anisotropic) materials—including the most probable orientation of critical flaws for offset uniaxial loads with strength anisotropy. The author anticipates that this information could be used to determine anisotropic stiffness degradation or anisotropic damage evolution for individual brittle (or quasi-brittle) composite-material constituents within finite-element or micromechanics-based software.

1.0 Introduction

The term "unit sphere" as used herein refers to the models that were developed by Batdorf and Crose (1974), Batdorf and Heinisch (1978), Evans (1978), and Matsuo (1981) to predict the probability of failure of brittle materials under multiaxial loading. These models use a unit radius sphere representing the random orientation of flaws to calculate the effect of multiaxial stresses on material reliability. This approach assumes that the strength-controlling flaws are randomly oriented, noninteracting planar micro-cracks of specified geometry but of variable size. Fracture mechanics relationships for mixed-mode (modes I, II, and III) crack growth—combined with the weakest-link theory and integration over the surface area of a unit radius sphere representing all possible orientations of microcracks—are used to calculate the material probability of failure.

This unit-sphere methodology was originally introduced within a statistical theory of brittle material strength by Weibull (1939), though without consideration for the mechanics of crack growth. Nemeth (2013) extended this methodology to predict anisotropic (transversely isotropic) brittle material strength response and demonstrated how this could be used as a failure criterion inside finite-element (or alternatively, micromechanics-based) software codes for individual brittle (or quasi-brittle) composite-material constituents to predict the overall strength response.

The unique feature of the unit-sphere methodology is the assumption that the presence of flaws in a brittle material drives the failure response and that these flaws are microcracks with an assumed orientation and geometry. In this manner, the stochastic strength response of the material can be predicted for an arbitrary multiaxial stress state. An interesting consequence of this methodology is that the orientation of the critical flaws (the failure-initiating flaws) relative to the applied multiaxial stress state can be predicted as a probabilistic distribution.

This report develops the generalized formulation to describe the probability density distribution (PDD) of the orientation of critical-strength-controlling flaws for the unit-sphere model. The derivation starts from the most basic level with the description of the weakest link mechanism and the Weibull

distribution. Following that is the description of the Batdorf unit-sphere methodology for the isotropic strength response. The extensions for the unit-sphere methodology with the anisotropic (transversely isotropic) strength response are provided to complete the description of all relevant parameters. These extensions are for (1) flaw orientation anisotropy, where a preexisting microcrack has a higher likelihood of being oriented in one direction than another direction, and (2) critical strength or fracture toughness anisotropy, where the level of critical strength σ_{Ic} or fracture toughness K_{Ic} for mode I crack propagation changes with the orientation to the microstructure (for a tensile mode of failure only). This leads to the generalized formulation for the PDD of the critical flaw orientation over the unit sphere. Examples are provided to demonstrate this methodology for isotropic and anisotropic materials for various stress states and off-axis loading.

If one knows the orientation distribution of critical flaws (and the subsequent direction of crack propagation), the anisotropic stiffness degradation (the anisotropic elastic constants associated with the damaged material) can be determined. The author anticipates that this will be helpful for a follow-on phase of this effort, not described here, of enabling the unit-sphere failure criterion methodology to work with NASA's micromechanics analysis code/generalized method of cells (MAC/GMC) (Bednarcyk and Arnold (2002)), which is based on the GMC family of micromechanics theories, including doubly and triply periodic versions of the GMC (Aboudi (1995)) and the High-Fidelity Generalized Method of Cells (HFGMC) (Aboudi et al. (2003)). This incorporation will allow the full exercise of the unit-sphere methodology, including incremental time/load steps and fatigue analysis (as described in Nemeth et al. (2005)), to predict the durability (strength and lifetime) of composite laminates and woven composite structures.

The unit-sphere methodology provides an improved mechanistic basis to the problem of predicting the strength response of an anisotropic material under multiaxial loading in comparison to polynomial interaction equation formulations such as Tsai-Wu, Tsai-Hill, and Hashin, among others. A unique physical attribute of this model is the ability to predict the critical-flaw-angle distribution for an arbitrary stress state. This distribution is derived and demonstrated in this report.

2.0 Model Description

2.1 Weibull Distribution

Consider a stressed component containing many flaws (microcracks), and assume that failure is due to any number of independent and mutually exclusive mechanisms (links). Each link involves an infinitesimal probability of failure. Discretize the component into n incremental links. The probability of survival $(P_{sV})_i$ of the i^{th} link is related to the probability of failure $(P_{fV})_i$ of the i^{th} link by $(P_{sV})_i = [1 - (P_{fV})_i]$, and the resultant probability of survival of the whole structure is the product of the individual probabilities of survival:

$$P_{sV} = \prod_{i=1}^{n} \left(P_{sV}\right)_i = \prod_{i=1}^{n} \left[1 - \left(P_{fV}\right)_i\right] \cong \prod_{i=1}^{n} \exp\left[-\left(P_{fV}\right)_i\right] = \exp\left[-\sum_{i=1}^{n}\left(P_{fV}\right)_i\right] \tag{1}$$

where the subscript V denotes volume-dependent terms. Equation (1) arises from the approximation to the exponential series

$$e^x = 1 + x + \frac{x^2}{2!} + \frac{x^3}{3!} + \frac{x^4}{4!} + \ldots \quad \text{(for all real values of } x\text{)} \tag{2}$$

where $(P_{fV})_i$ is assumed to be a small number such that the higher order terms in Equation (2) can be neglected.

Assume the existence of a function $\eta_V(\sigma)$, referred to as the crack-density function, representing the number of flaws per unit volume that have a strength equal to or less than σ. Under a local tensile stress σ_i, the probability of failure of the i^{th} link, representing the incremental volume ΔV_i, is

$$\left(P_{fV}\right)_i = \left[\eta_V(\sigma_i)\, \Delta V_i\right] \tag{3}$$

where the incremental volume ΔV_i is arbitrarily small such that the value of the expression within the brackets is much less than one. If one applies a uniform tensile stress σ, such that $\sigma = \sigma_i$ for all incremental volumes ΔV_i, then from Equation (1) the resultant probability of survival for material volume V, where V is the sum of all ΔV_i, is

$$P_{sV} = \exp[-\eta_V(\sigma)V] \tag{4}$$

Equation (4) can also be derived from the Poisson probability density function. This distribution is described by (see Hoel et al. (1971), for example)

$$P(X = x) = f(x) = \begin{cases} \dfrac{\lambda^x \exp(-\lambda)}{x!} & x = 0,1,2, \ldots \\ 0 & \text{elsewhere} \end{cases} \tag{5}$$

where λ is a positive number. The real-valued function $f(x)$ is the discrete density function of random variable X where $P(X = x)$ is the probability that a discrete real-valued random variable X equals a possible value x. The Poisson distribution approximates the binomial distribution for large values of n, where n is the number of Bernoulli trials with success probability $p = \lambda/n$ at each trial. Equation (4) is obtained when $P(X = 0)$ is computed for $n = V$ and $p = \eta_V(\sigma)$; hence,

$$P_{sV} = P(X = 0) = \frac{\lambda^0 \exp(-\lambda)}{0!} = \exp(-\lambda) = \exp\left[-\eta_V(\sigma)V\right] \tag{6}$$

Equation (6) calculates the probability that no flaws of strength σ or less are present in the material volume V and, therefore, represents the survival probability of the material under applied load σ.

The probability of failure for the uniformly stressed volume V is

$$P_{fV} = 1 - \exp\left[-\eta_V(\sigma)V\right] \tag{7}$$

where V is the total volume.

Weibull introduced a three-parameter power function for the crack-density function $\eta_V(\sigma)$:

$$\eta_V(\sigma) = \left(\frac{\sigma - \sigma_{uV}}{\sigma_{oV}}\right)^{m_V} \tag{8}$$

where σ_{uV} is the threshold stress parameter. The scale parameter σ_{oV} then corresponds to the stress level where 63.21 percent of tensile specimens with unit volumes would fracture. The scale parameter has dimensions of stress × (volume)$^{1/m_V}$, where m_V is the shape parameter (Weibull modulus)—a dimensionless parameter that measures the degree of strength variability. As m_V increases, the dispersion decreases. The threshold stress parameter σ_{uV} is usually taken as zero for brittle materials (ceramics and glasses). This parameter is the value of the applied stress below which the failure probability is zero. When this parameter is zero, the two-parameter Weibull model is obtained in Equation (7). The two-parameter crack-density function is expressed as

$$\eta_V(\sigma) = \left(\frac{\sigma}{\sigma_{oV}}\right)^{m_V} = k_{wV}\,\sigma^{m_V} \tag{9}$$

where $k_{wV} = (\sigma_{oV})^{-m_V}$ is the uniaxial Weibull crack-density coefficient (for an applied uniaxial load).

2.2 Batdorf Unit-Sphere Model for Isotropic Strength Response

Batdorf and Crose (1974) propose a statistical theory in which attention is focused on cracks and their failure under stress. Flaws (assumed to be microcracks in shape and size) are taken to be uniformly distributed and randomly oriented in the material bulk. Fracture is assumed to depend only on the tensile stress acting normal to the crack plane; hence, shear insensitivity is inherent to this first model. Subsequently, Batdorf and Heinisch (1978) included the detrimental effects of shear traction on a flaw plane. Their method applies fracture mechanics concepts by combining the crack geometry and a mixed-mode fracture criterion to describe the condition for crack growth.

In the Batdorf unit-sphere theory, the incremental failure probability ΔP_{fV} under an applied multiaxial state of stress Σ at a given location in the component can be described as the product of two probabilities:

$$\Delta P_{fV}\left(\Sigma, \sigma_{\mathrm{I}eqc}, \Delta V\right) = \Delta P_{1V} P_{2V} \tag{10}$$

where ΔP_{1V} is the probability of the existence in incremental volume ΔV of a crack having an *equivalent*, or effective, critical stress between $\sigma_{\mathrm{I}eqc}$ and $\sigma_{\mathrm{I}eqc} + \Delta\sigma_{\mathrm{I}eqc}$. Critical stress $\sigma_{\mathrm{I}c}$ is defined as the remote, uniaxial fracture strength of a material containing a given crack in mode I loading. The term $\sigma_{\mathrm{I}eqc}$ denotes an effective (or equivalent) critical mode I stress from applied multiaxial stresses. The second probability, P_{2V}, denotes the probability that a crack of critical stress $\sigma_{\mathrm{I}eqc}$ will be oriented in a direction such that an effective stress $\sigma_{\mathrm{I}eq}$ (which is a function of fracture criterion, stress state, and crack configuration) satisfies the condition $\sigma_{\mathrm{I}eq} \geq \sigma_{\mathrm{I}eqc}$. The effective stress $\sigma_{\mathrm{I}eq}$ is defined as the equivalent mode I stress that a flaw would experience when subjected to a multiaxial stress state that results in mode I, II, and III crack surface displacements, and $\sigma_{\mathrm{I}eqc}$ is the threshold value of $\sigma_{\mathrm{I}eq}$ where unstable catastrophic crack growth ensues. An incremental volume ΔV is used in Equation (10) because an infinitesimal volume $\mathrm{d}V$ cannot enclose a crack of critical stress $\sigma_{\mathrm{I}eqc}$ and associated critical crack length a_c.

The effective stress $\sigma_{\mathrm{I}eq}$ represents an equivalent normal stress on the crack face from the combined action of the normal stress σ_n and the shear stress τ. The microcrack orientation is defined by the angular coordinates α and β, where the direction normal to the plane of the microcrack is specified by the radial line defined by α and β in space (see Fig. 1(a)). For the sake of brevity, the development of the effective stress equations is not shown (for details, see Nemeth et al. (2003, 2005)). For a tensile mode of failure assuming a penny-shaped crack with the Shetty mixed-mode fracture criterion (Shetty (1987)), the effective stress becomes

$$\sigma_{\mathrm{I}eq} = \frac{1}{2}\left\{\sigma_n + \sqrt{\sigma_n^2 + \left[\frac{4\tau}{\overline{C}\left(2-\nu\right)}\right]^2}\right\} \tag{11}$$

where ν is Poisson's ratio and $\overline{C}$ is the Shetty shear-sensitivity coefficient, with values typically in the range $0.80 \leq \overline{C} \leq 2.0$. As $\overline{C}$ increases, the response becomes progressively more shear insensitive. Shear increases the equivalent stress as shown in Equation (11), and this has a deleterious effect on the predicted material strength. For a penny-shaped crack with a material having a Poisson's ratio $\nu \sim 0.22$ and $\overline{C} = 0.80$, 0.85, 1.05, and 1.10, Equation (11) approximates, respectively, the following criteria: Ichikawa's maximum energy-release-rate approximation (Ichikawa (1991)), the maximum tangential stress (Erdogan and Sih (1963)), the maximum strain-energy-release-rate formulation of Hellen and Blackburn (1975), and colinear crack extension. The value of $\overline{C}$ also can be fit empirically to experimental data—either on introduced cracks (as is done in Shetty (1987)) or on specimens being tested multiaxially.

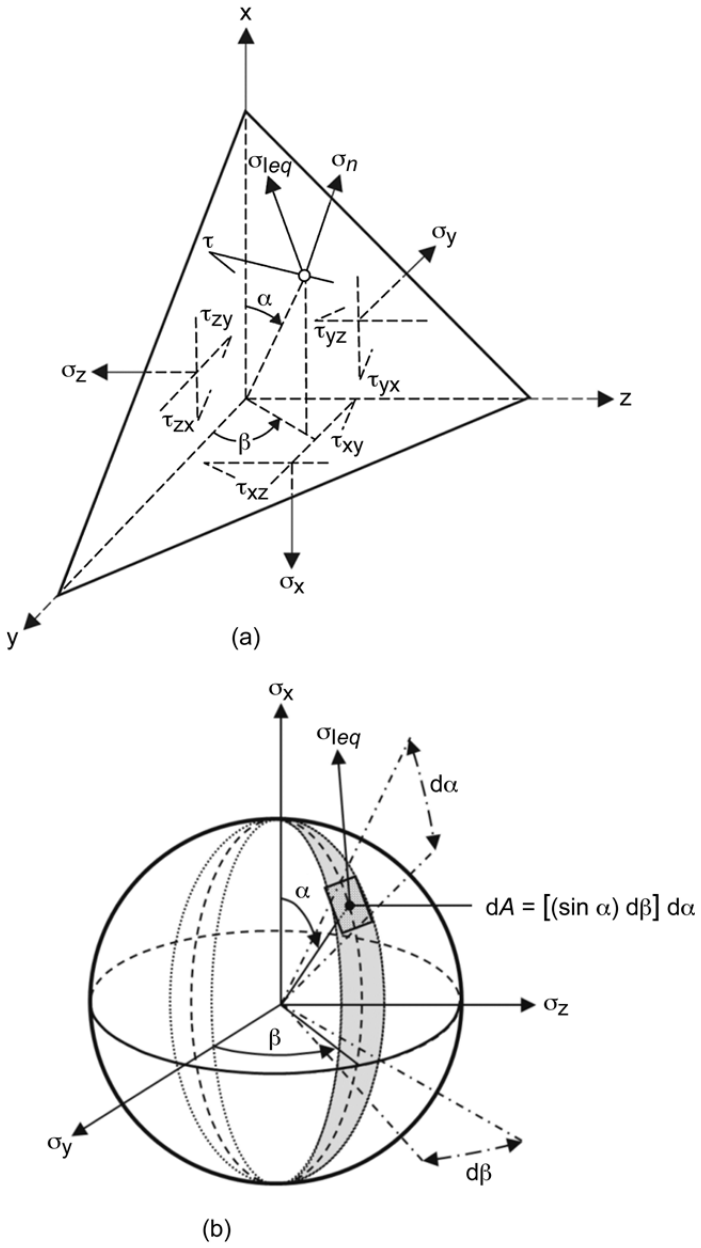

Figure 1.—Projection of equivalent stress onto a unit radius sphere. (a) Cauchy stress components on an infinitesimal tetrahedron resolving a normal stress, σ_n, and a resultant shear stress, τ, on a plane normal to the direction defined by angular coordinates α and β. (b) Projection of equivalent stress onto a unit radius sphere in the global coordinate system. The unit radius sphere represents all possible flaw orientations, where σ_{leq} is an equivalent (or effective) stress; σ_x, σ_y, and σ_z are normal orthogonal stress components; and τ_{xy}, τ_{yz}, and τ_{zx} are shear stress components. An infinitesimal area, dA, on the unit sphere represents a particular flaw orientation (a direction normal to the flaw plane), and σ_{leq} is a function of σ_n and τ for an assumed crack shape and multiaxial fracture criterion.

A material is assumed to have n individual failure modes. Material reliability (probability of survival) is assumed to be the product of the survival probability of all of the failure modes. These failure modes can be from different flaw populations, from the flaws associated with different material constituents (i.e., composites as described in Nemeth (2013)), or from different physical mechanisms that govern the material failure such as tensile loading versus compressive loading. Here the compressive mode of failure is assumed to be of a different nature than the tensile failure mode—possibly involving the interaction of arrested cracks (flaws with initial crack growth that subsequently stops because of the angle of the crack growth and the interaction with the local stress field). Regardless, the Weibull distribution here is assumed to describe the stochastic strength response phenomenologically. This is argued further in Nemeth and Bratton (2011). The compressive failure mode is assumed to be controlled by shear stress, and a simple Tresca-like effective stress σ_{1eq} relation can be prescribed as

$$\sigma_{1eq} = 2\tau \tag{12}$$

The multiplier of 2 in Equation (12) was chosen so that the maximum effective stress on the unit sphere in pure uniaxial compression is equal to the applied compressive stress. When the normal stress component σ_n on the crack face is tensile, then the value of σ_{1eq} in Equation (12) is set to zero in the unit sphere evaluation. A more rigorous treatment to account for compression would include the frictional effects of the opposed crack surfaces in contact in the effective stress relation. However, Equation (12) is sufficient for the demonstration purposes of this report.

2.2.1 Relationship of Crack Probability of Occurrence ΔP_{1V} to the Crack-Density Function η_V

The strength of a component containing a flaw population is related to the critical flaw size, which is used implicitly in statistical fracture theories. Batdorf and Crose (1974) describe the crack probability of occurrence ΔP_{1V} as

$$\Delta P_{1V} = \Delta V \frac{d\eta_V\left(\sigma_{1eqc}\right)}{d\sigma_{1eqc}} d\sigma_{1eqc} \tag{13}$$

This is better understood using Figure 2. In Figure 2(a), for example, a point on the curve $\eta_V(\sigma_{1eqc})\Delta V$ for the value $\sigma_{1eqc,1}$ represents the number of flaws in ΔV having a strength equal to or less than $\sigma_{1eqc,1}$. Then, from Figure 2(a),

$$\begin{aligned}
&\eta_V(\sigma_{1eqc,2})\Delta V - \eta_V(\sigma_{1eqc,1})\Delta V \\
&\quad = \text{Probability that a flaw of strength } \sigma_{1eqc,2} \text{ or less is in } \Delta V \\
&\qquad\qquad - \text{Probability that a flaw of strength } \sigma_{1eqc,1} \text{ or less is in } \Delta V \\
&\quad = \text{Probability that a flaw of strength between } \sigma_{1eqc,1} \text{ and } \sigma_{1eqc,2} \text{ is in } \Delta V
\end{aligned} \tag{14}$$

Equivalently in Figure 2(b),

$$\begin{aligned}
&[\eta_V(\sigma_{1eqc}) + d\eta_V]\Delta V - \eta_V(\sigma_{1eqc})\Delta V \\
&\quad = \text{Probability that a flaw of strength } (\sigma_{1eqc} + d\sigma_{1eqc}) \text{ or less is in } \Delta V \\
&\qquad\qquad - \text{Probability that a flaw of strength } \sigma_{1eqc} \text{ or less is in } \Delta V \\
&\quad = \text{Probability that a flaw of strength between } \sigma_{1eqc} \text{ and } (\sigma_{1eqc} + d\sigma_{1eqc}) \text{ is in } \Delta V \\
&\quad = \Delta V\, d\eta_V
\end{aligned} \tag{15}$$

The slope s of the relation $\eta_V(\sigma_{1eqc})\,\Delta V$ is $s = (d\eta_V / d\sigma_{1eqc})\,\Delta V$ as shown in Figure 2(b); therefore, multiplying the slope s by $d\sigma_{1eqc}$ yields the result of Equation (13).

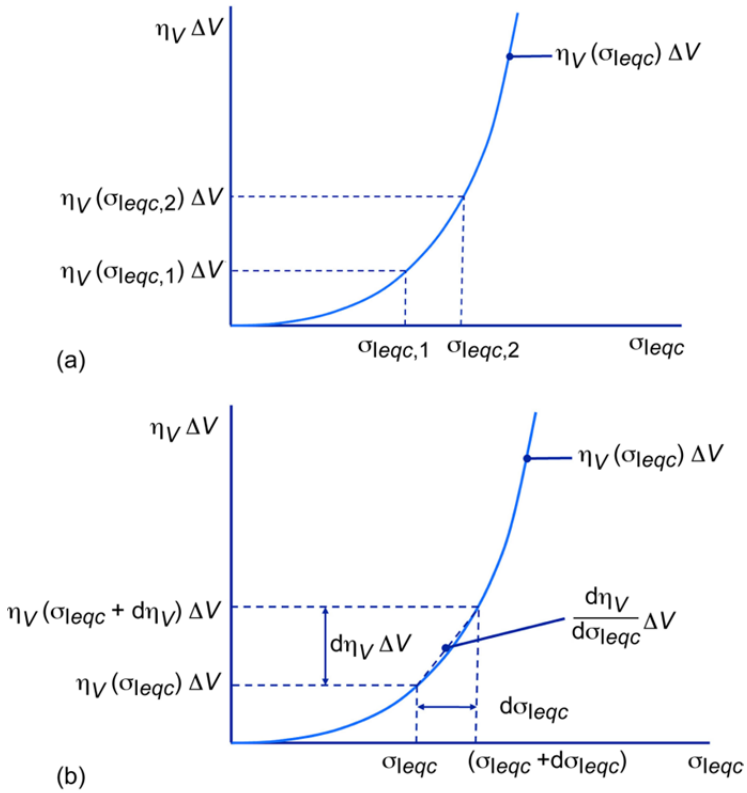

Figure 2.—Crack-density function, η_V, versus the critical equivalent stress, σ_{Ieqc}, where ΔV is incremental volume, shown to explain Equation (13). (a) Incremental differences in values. (b) The same differences described in terms of infinitesimal values.

2.2.2 Random Flaw Orientation as Described by a Unit Sphere

The term P_{2V} shown in Equation (10) is expressed as

$$P_{2V} = \frac{\Omega\left(\Sigma, \sigma_{Ieqc}\right)}{4\pi} \tag{16}$$

where $\Omega(\Sigma, \sigma_{Ieqc})$ is the area of the solid angle projected onto the unit radius sphere in stress space (see Fig. 1(b)) containing all the crack orientations for which $\sigma_{Ieq} \geq \sigma_{Ieqc}$ for the applied far-field multiaxial stress state Σ. The infinitesimal area, dA, on the unit sphere represents a particular flaw orientation (a direction normal to the flaw plane), and σ_{Ieq} is an equivalent stress, which is a function of an assumed crack shape and multiaxial fracture criterion. The constant 4π is the surface area of a unit radius sphere and corresponds to a solid angle containing all possible flaw orientations. Equation (16) assumes that the flaws are randomly oriented with a uniform distribution (equal likelihood of being oriented at any angles α and β). If it is assumed that the other properties like crack geometry and K_{Ic} are also independent of α and β, the strength response becomes isotropic (independent of the applied direction of load).

2.2.3 Unit-Sphere Failure Probability Formulation for Isotropy

Integrating Equation (10) with respect to σ_{Ieqc} and using Equation (4) yields the probability of survival of a (uniformly stressed) volume element ΔV_i:

$$\left(P_{sV}\right)_i = \exp\left\{-\Delta V\left[\int_0^{\sigma_{I eq,\max}} \frac{\Omega\left(\Sigma,\sigma_{I eqc}\right)}{4\pi}\frac{\mathrm{d}\,\eta_V\left(\sigma_{I eqc}\right)}{\mathrm{d}\,\sigma_{I eqc}}\mathrm{d}\,\sigma_{I eqc}\right]\right\}_i \tag{17}$$

where $\sigma_{I eq,\max}$ is the maximum effective stress that a randomly oriented flaw could experience from the given stress state. Hence, integrating over the entire volume of the component results in the failure probability:

$$P_{fV} = 1-\exp\left\{-\int_V\left[\int_0^{\sigma_{I eq,\max}} \frac{\Omega\left(\Sigma,\sigma_{I eqc}\right)}{4\pi}\frac{\mathrm{d}\,\eta_V\left(\sigma_{I eqc}\right)}{\mathrm{d}\,\sigma_{I eqc}}\mathrm{d}\,\sigma_{I eqc}\right]\mathrm{d}\,V\right\} \tag{18}$$

where $\sigma_{I eq,\max}$ is the maximum effective stress that a randomly oriented flaw could experience in the component and Σ is allowed to vary within the component.

Because of the effect of multiaxial stress states, the crack-density function $\eta_V(\sigma_{I eqc})$ is altered in the Batdorf formulation. Batdorf and Heinisch, (1978) have typically used a power-law formulation for $\eta_V(\sigma_{I eqc})$, which leads to the Batdorf crack-density function of the form

$$\eta_V\left(\sigma_{I eqc}\right) = k_{BV}\sigma_{I eqc}^{m_V}(\mathrm{x},\mathrm{y},\mathrm{z},\alpha,\beta) = \frac{\bar{k}_{BV}\sigma_{I eqc}^{m_V}(\mathrm{x},\mathrm{y},\mathrm{z},\alpha,\beta)}{\sigma_{oV}^{m_V}} \tag{19}$$

where x, y, and z correspond to the location within the component and α and β are the unit-sphere orientation angles. The term k_{BV} is the Batdorf crack-density coefficient, and $\bar{k}_{BV}$ is the normalized Batdorf crack-density coefficient whereby $\bar{k}_{BV} = k_{BV}/k_{wV}$ as described in Nemeth et al. (2003, 2005). The material Batdorf crack-density coefficient k_{BV} and the Weibull modulus m_V are evaluated from experimental inert strength fracture data. By convention, $\bar{k}_{BV}$ is calibrated to a uniaxial stress state. Batdorf and Crose (1974) initially proposed a Taylor series expansion for $\eta_V(\sigma_{I eqc})$, but this method has computational difficulties. Note that $\eta_V(\sigma_{I eqc})$ has units of inverse volume.

Although the Weibull (Eq. (9)) and Batdorf (Eq. (19)) crack-density functions are similar in form, they are not the same. The Weibull function simply depends on the applied uniaxial stress distribution σ and is the only term other than m_V and the volume necessary to calculate P_{fV}. It does not extrapolate to other multiaxial stress states. The Batdorf function depends on the equivalent mode I strength of the crack $\sigma_{I eqc}$, which is probabilistic and must be integrated over a range of values for a given stress state. Furthermore, to obtain P_{fV}, a crack orientation function, P_{2V}, must be considered in addition to the density function and the volume. Finally, the Batdorf coefficient k_{BV} cannot be calculated from inert strength data until a fracture criterion and crack shape are chosen—in contrast to the Weibull coefficient k_{wV}, which depends only on normalizing or calibrating to experimental rupture data.

To determine a component probability of failure, one must evaluate P_{2V} (Eq. (16)) for each elemental volume ΔV_i, within which a uniform multiaxial stress state Σ is assumed. The solid angle $\Omega(\Sigma, \sigma_{I eqc})$ depends on the selected fracture criterion, the crack configuration, and the applied stress state. For multiaxial stress states, with few exceptions, $\Omega(\Sigma, \sigma_{I eqc})$ must be determined numerically. For a sphere of unit radius (see Fig. 1(b)), an elemental surface area of the sphere is $\mathrm{d}A = \sin\alpha\,\mathrm{d}\beta\,\mathrm{d}\alpha$. If we project onto the spherical surface the equivalent (effective) stress $\sigma_{I eq}(\Sigma, \alpha, \beta)$, the solid angle $\Omega(\Sigma, \sigma_{I eqc})$ will be the area of the sphere containing all the projected equivalent stresses satisfying $\sigma_{I eq} \geq \sigma_{I eqc}$. Note that the symmetry of $\sigma_{I eq}$ means that only one-eighth of the unit sphere needs to be integrated for an isotropic strength response. However, for transverse isotropy, one-half of the sphere should be integrated. When one-half of the unit sphere is considered,

$$\frac{\Omega\left(\Sigma,\sigma_{\mathrm{I}eqc}\right)}{4\pi}=\left(\frac{1}{2\pi}\right)\int_0^{2\pi}\int_0^{\pi/2}H\left(\sigma_{\mathrm{I}eq},\sigma_{\mathrm{I}eqc}\right)\sin\alpha\ \mathrm{d}\alpha\ \mathrm{d}\beta \tag{20}$$

where

$$H(\sigma_{\mathrm{I}eq},\ \sigma_{\mathrm{I}eqc})=1 \qquad \sigma_{\mathrm{I}eq}\geq\sigma_{\mathrm{I}eqc}$$

$$H(\sigma_{\mathrm{I}eq},\ \sigma_{\mathrm{I}eqc})=0 \qquad \sigma_{\mathrm{I}eq}<\sigma_{\mathrm{I}eqc}$$

The Heaviside function $H(\sigma_{\mathrm{I}eq},\ \sigma_{\mathrm{I}eqc})$ is a function of fracture criterion, stress state, crack configuration, and crack orientation. Substituting into Equation (18) and integrating first with respect to $\sigma_{\mathrm{I}eqc}$ for each individual angle α or β on the unit sphere changes the component failure probability to (Batdorf (1978a,b))

$$P_{fV}=1-\exp\left[-\frac{1}{2\pi}\int_V\int_0^{2\pi}\int_0^{\pi/2}\eta_V\left(\sigma_{\mathrm{I}eq}\right)\sin\alpha\ \mathrm{d}\alpha\ \mathrm{d}\beta\ \mathrm{d}V\right] \tag{21}$$

where

$$\eta_V\left(\sigma_{\mathrm{I}eq}\right)=k_{BV}\,\sigma_{\mathrm{I}eq}^{m_V}\left(\mathrm{x},\mathrm{y},\mathrm{z},\alpha,\beta\right)$$

For a given incremental volume, $\sigma_{\mathrm{I}eq}(\mathrm{x},\ \mathrm{y},\ \mathrm{z},\ \alpha,\ \beta)$ is the projected equivalent stress over the unit radius sphere in coordinate stress space as shown in Figure 1.

Equation (21) circumvents the involved numerical integration of $\Omega(\Sigma,\ \sigma_{\mathrm{I}eqc})$ as was originally developed in Nemeth et al. (1990). Equations (18) and (21) are equivalent formulations; however, Equation (21) is more convenient for computational purposes with the few exceptions where special-case closed-form solutions exist for particular stress states, crack geometries, and fracture criteria.

2.3 Unit-Sphere Model for Transversely Isotropic Strength Response

Two different physical mechanisms were considered in order to extend the unit-sphere model to account for anisotropic strength response: (1) flaw orientation anisotropy, whereby a preexisting microcrack has a higher likelihood of being oriented in one direction than another direction and (2) critical strength or fracture toughness anisotropy, whereby the level of critical strength $\sigma_{\mathrm{I}c}$ or fracture toughness $K_{\mathrm{I}c}$ for mode I crack propagation changes with regard to the orientation of the microstructure (for a tensile mode of failure only). Flaw orientation anisotropy was previously considered by Buch et al. (1977), and critical strength anisotropy was previously considered by Batdorf (1973). Both models were developed to simulate the graphite anisotropic strength response. Extensions to these models, described and demonstrated in Nemeth (2013) for transversely isotropic strength response, are reproduced herein because terms from these formulations are used in the flaw orientation probability density function (PDF) formulation. The extensions include shear sensitivity for flaws and an improved functional form for the anisotropy equations.

2.3.1 Flaw Orientation Anisotropy

Flaw orientation anisotropy refers to the situation where a flaw has a higher likelihood of being oriented in one direction than another for a given critical strength. This means that a material will be stronger on average in one direction than another. An isotropic brittle material is equally strong in any direction, and thus its flaws are uniformly randomly oriented. However, in components made by processes such as extrusion or hot pressing, which induce texture, a bias will exist in the orientation distribution of processing flaws. Also, components finished by surface grinding will contain machining

damage in the form of surface cracks that are oriented parallel and transverse to the grinding direction. In composite materials, the interface or interfacial layer between the fiber and the matrix can act as a flaw with an orientation bias that induces an anisotropic strength response.

In the following unit-sphere formulation, consideration is given to a flaw that has a higher likelihood of being oriented in one direction than another. If an argument analogous to Equation (10) is used, the incremental probability of failure under the applied multiaxial state of stress Σ for a given α and β orientation of the (direction or vector) normal to the particular flaw plane can be written as the product of two probabilities:

$$\Delta P_{fV}(\Sigma, \alpha, \beta, \sigma_{\mathrm{I}eqc}, \Delta V) = \Delta P_{1V}\ \wp(\alpha, \beta)\, d\alpha\, d\beta\, H(\sigma_{\mathrm{I}eq}, \sigma_{eqc}) \tag{22}$$

where ΔP_{1V} is the probability that a crack having an equivalent critical stress between $\sigma_{\mathrm{I}eqc}$ and $\sigma_{\mathrm{I}eqc} + d\sigma_{\mathrm{I}eqc}$ exists in an incremental volume element ΔV. The second probability, $\wp(\alpha, \beta)\, d\alpha\, d\beta$, denotes the probability that a crack of critical stress $\sigma_{\mathrm{I}eqc}$ is oriented in the range between α and $(\alpha + d\alpha)$ and between β and $(\beta + d\beta)$, where the orientation of the microcrack is described by the vector that is normal to the plane of the microcrack. The Heaviside function $H(\sigma_{\mathrm{I}eq}, \sigma_{\mathrm{I}eqc})$ is identical to that as defined in Equation (20), where $H(\sigma_{\mathrm{I}eq}, \sigma_{\mathrm{I}eqc}) = 1$ when $\sigma_{\mathrm{I}eq}(\Sigma, \alpha, \beta) \geq \sigma_{\mathrm{I}eqc}$ and where $H(\sigma_{\mathrm{I}eq}, \sigma_{\mathrm{I}eqc}) = 0$ when $\sigma_{\mathrm{I}eq}(\Sigma, \alpha, \beta) < \sigma_{\mathrm{I}eqc}$. The effective stress $\sigma_{\mathrm{I}eq}(\Sigma, \alpha, \beta)$ is defined as the equivalent mode I stress oriented at coordinates α and β that a flaw would experience when subjected to a multiaxial stress state Σ that results in mode I, II, and III crack surface displacements, and $\sigma_{\mathrm{I}eqc}$ is the threshold value of $\sigma_{\mathrm{I}eq}$ where unstable catastrophic crack growth ensues.

Analogous to Equations (16) and (20) for the unit sphere,

$$P_{2V} = \int_0^{2\pi} \int_0^{\pi/2} \wp(\alpha,\beta) H\left(\sigma_{\mathrm{I}eq}, \sigma_{\mathrm{I}c}\right) \sin\alpha\, d\alpha\, d\beta \tag{23}$$

where

$$\wp(\alpha,\beta) = \frac{\zeta(\alpha,\beta)}{\int_0^{2\pi} \int_0^{\pi/2} \zeta(\alpha,\beta)\ \sin\alpha\, d\alpha\, d\beta} \tag{24}$$

and

$$H(\sigma_{\mathrm{I}eq}, \sigma_{\mathrm{I}c}) = 1 \qquad \sigma_{\mathrm{I}eq} \geq \sigma_{\mathrm{I}c}$$

$$H(\sigma_{\mathrm{I}eq}, \sigma_{\mathrm{I}c}) = 0 \qquad \sigma_{\mathrm{I}eq} < \sigma_{\mathrm{I}c}$$

Equation (24) is explained further in Section 2.4. The function $\zeta(\alpha, \beta)$ describes the degree of anisotropy of the flaw orientation, where the normal direction to the flaw plane is given by angles α and β.

Equations (23) and (24) modify Equation (21) for probability of failure:

$$P_{fV} = 1 - \exp\left[- \int_V \int_0^{2\pi} \int_0^{\pi/2} \wp(\alpha,\beta)\ \eta_V\left(\sigma_{\mathrm{I}eq}\right)\ \sin\alpha\, d\alpha\, d\beta\, dV \right] \tag{25}$$

where

$$\eta_V\left(\sigma_{1eq}\right) = k_{BV}\,\sigma_{1eq}^{m_V}\left(x,y,z,\alpha,\beta\right) = \bar{k}_{BV}\left(\frac{\sigma_{1eq}^{m_V}\left(x,y,z,\alpha,\beta\right)}{\sigma_{oV}}\right)^{m_V}$$

The normalized crack-density coefficient $\bar{k}_{BV}$ now includes the effect of flaw orientation anisotropy and is evaluated numerically from Equation (25) for a uniaxial stress state applied in one of the material coordinate system axis directions.

For a transversely isotropic strength response, ζ in Equation (24) is only a function of α. Buch et al. (1977) introduced a cosine power function for $\zeta(\alpha) = [\cos(\alpha)]^{\phi}$ where ϕ is a constant. This relation was modified in Nemeth (2013) to enhance the functional flexibility and is expressed as

$$\left.\begin{aligned} \zeta(\alpha) &= \left[\cos\left(\frac{\alpha\pi}{2\Lambda_L}\right)\right]^{\phi_L} && 0 \le \alpha \le \Lambda_L \\ \zeta(\alpha) &= 0 && \Lambda_L < \alpha \le \frac{\pi}{2} \end{aligned}\right\} \tag{26}$$

Alternatively,

$$\left.\begin{aligned} \zeta(\alpha) &= 0 && 0 \le \alpha < \frac{\pi}{2} - \Lambda_T \\ \zeta(\alpha) &= \left(\sin\left\{\frac{\pi}{2\Lambda_L}\left[\alpha - \left(\frac{\pi}{2} - \Lambda_T\right)\right]\right\}\right)^{\phi_T} && \text{for} \quad \frac{\pi}{2} - \Lambda_T \le \alpha \le \frac{\pi}{2} \end{aligned}\right\} \tag{27}$$

where Λ and ϕ are constants (with subscripts L or T) that control the degree of anisotropy, and $0 < \Lambda \le \pi/2$ and $\phi \ge 0$. When $\Lambda = \pi/2$ and $\phi = 0$, the isotropic strength response is obtained. Equations (26) and (27) are defined for one-half of the unit sphere (the top half, as shown in Fig. 1(b) where $0 \le \alpha \le \pi/2$). Referring to Figure 3, Equation (26) represents the "polar-cap" or longitudinal L distribution of flaws and Equation (27) represents an "equatorial-belt" or transverse T distribution of flaws. The polar-cap distribution describes crack planes that are distributed symmetrically (centered) about a plane (in this case, the σ_y–σ_z plane), and the equatorial-belt distribution describes crack planes that are distributed symmetrically (centered) along a line (in this case the σ_x axis). For the polar-cap distribution, $\bar{k}_{BV}$ is evaluated for a uniaxial stress along the σ_x direction; and for the equatorial-belt distribution, it is evaluated in the σ_y (or optionally the σ_z) direction.

The separate polar-cap and equatorial-belt distributions are introduced to describe individual and distinctly different failure modes. For a unidirectional fiber-reinforced composite, the polar cap can be used to represent the fiber strength distribution and the equatorial belt can be used to represent the matrix-fiber interface. The equatorial-belt and the polar-cap distributions can be considered to equivalently represent global failure planes, which are referred to as "action planes" in the Puck multiaxial strength model for composites (see Lutz (2006) for a description). The angular width of the belt or cap with regard

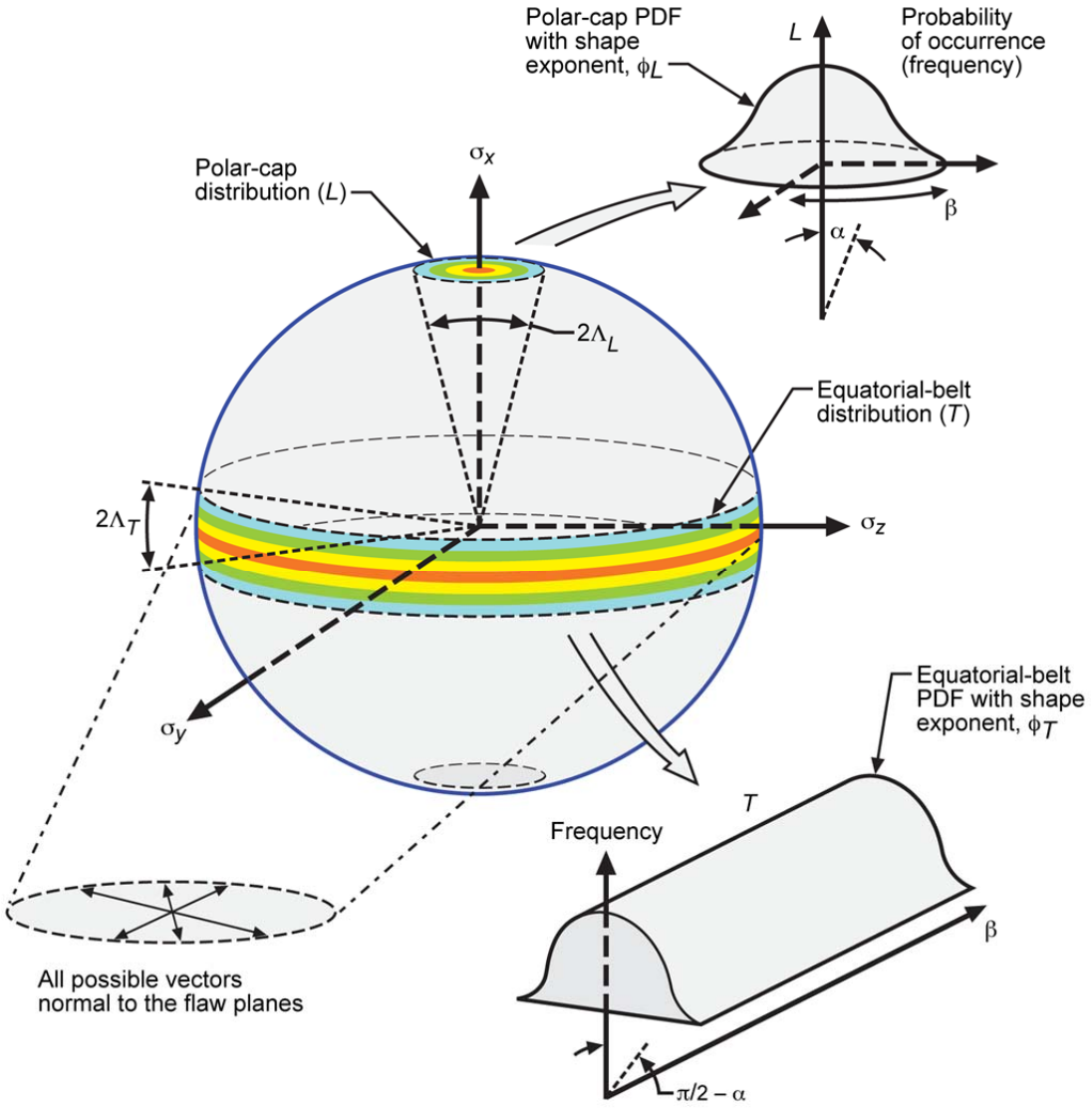

Figure 3.—Unit sphere with probability distribution functions (PDFs) describing the anisotropy of flaw orientation, where α and β are angular coordinates and Λ_L and Λ_T are constants in the flaw-orientation anisotropy function representing longitudinal and transverse distributions. Orientation is described with the normal to the crack plane. In this figure, two orientation functions are described: (1) a polar-cap distribution describing crack planes distributed symmetrically (centered) about a plane (in this case the σ_y–σ_z plane) and (2) an equatorial-belt distribution where crack planes are distributed symmetrically (centered) along a line (in this case, the σ_x axis).

to angle α indicates the maximum extent of scatter of a flaw orientation. Flaws or action planes oriented outside of the scatter bands of the cap and belt are assumed to not exist or not contribute to the likelihood of failure. An example of this methodology is provided in Nemeth (2013) for a unidirectional polymer matrix composite (PMC) under biaxial loading.

2.3.2 Critical Strength or Stress Intensity Factor Anisotropy

Batdorf (1973) approached strength anisotropy using the σ_{Ic} strength ellipsoid approach (describing an ellipsoid rather than a unit sphere). This was applied to graphite—a mildly anisotropic material. In this report, strength anisotropy is used with the critical stress-intensity factor (fracture toughness) K_{Ic} varying with orientation angle on the unit sphere. This is functionally equivalent to σ_{Ic} varying with orientation, and it is also functionally equivalent to the size of the flaw changing with the orientation angle. With regard to a ceramic matrix composite (CMC), where failure from loading in the fiber direction is by matrix cracking with large-scale fiber bridging, fracture toughness cannot be defined on the global scale of the structure. In that case, one has to consider critical strength as a metric. However, it is acceptable to use fracture toughness on the local scale at the crack tip, where micromechanics can account for the bridging explicitly. In this report, fiber bridging is not considered directly. Of first-order importance herein is that local fracture toughness could change with the orientation of the flaw plane (or action plane) and the applied loading. The specific micromechanics of how this might occur is not considered here.

The modeling approach taken here is similar to that described previously for flaw-orientation anisotropy (Section 2.3.1). The critical strength σ_{Ic} is defined as the fracture strength of the crack in mode I loading and is proportional to K_{Ic}. Therefore, for anisotropic $K_{Ic}(\alpha, \beta) = (c\ \sigma_{Ic}(\alpha, \beta)) = \left[c\sigma_{Ic,\max} \bar{f}_{Ic}(\alpha,\beta) \right]$, where c is a constant ($c = Y\sqrt{a_c}$ with crack-shape geometry factor Y and critical crack length a_c), $\sigma_{Ic,\max}$ is the maximum value of σ_{Ic} over the unit sphere (for all α and β), and $\bar{f}_{Ic}(\alpha,\beta)$ is a normalized function expressing the degree of this anisotropy. The unit-sphere formulation described previously is used, except the Heaviside step function in Equations (20) and (23) is modified as follows:

$$\left.\begin{aligned} H\left(\sigma_{Ieq}, \sigma_{Ieqc}\right) &= 1 \qquad \frac{\sigma_{Ieq}}{\bar{f}_{Ic}(\alpha,\beta)} \geq \sigma_{Ieqc,\max} \\ H\left(\sigma_{Ieq}, \sigma_{Ieqc}\right) &= 0 \qquad \frac{\sigma_{Ieq}}{\bar{f}_{Ic}(\alpha,\beta)} < \sigma_{Ieqc,\max} \end{aligned}\right\} \tag{28}$$

where σ_{Ieqc} is substituted for σ_{Ic} to indicate generalized mixed-mode loading.

For a transversely isotropic response where anisotropy is only a function of angle α, the function $\bar{f}_{Ic}(\alpha)$ over the top half of the unit sphere ($0 \leq \alpha \leq \pi/2$) is arbitrarily defined for the L distribution as

$$\left.\begin{aligned} \bar{f}_{Ic}(\alpha) &= 1 - \left| \left(\frac{1}{2}\right) + \frac{1}{2}\cos\left(\frac{\alpha\pi}{\xi_L}\right) \right|^{\gamma_L} \left(1 - \frac{1}{r_L}\right) \qquad 0 \leq \alpha \leq \xi_L \\ \bar{f}_{Ic}(\alpha) &= 1 \qquad\qquad\qquad\qquad\qquad\qquad\qquad\qquad \xi_L < \alpha \leq \frac{\pi}{2} \end{aligned}\right\} \tag{29}$$

and for the T distribution

$$\left.\begin{aligned} \bar{f}_{Ic}(\alpha) &= 1 && 0 \le \alpha < \frac{\pi}{2} - \xi_T \\ \bar{f}_{Ic}(\alpha) &= 1 - \left| \left(\frac{1}{2}\right) + \frac{1}{2}\cos\left\{\frac{\pi}{\xi_T}\left[\alpha - \left(\frac{\pi}{2} - \xi_T\right)\right]\right\} + \pi \right|^{\gamma_T} \left(1 - \frac{1}{r_T}\right) && \frac{\pi}{2} - \xi_T \le \alpha \le \frac{\pi}{2} \end{aligned}\right\} \quad (30)$$

where ξ_L, ξ_T, γ_L, γ_T, r_L, and r_T are constants. The L subscript relates to the polar-cap strength anisotropy distribution for crack planes symmetrically distributed (centered) about a plane (in this case, the σ_y–σ_z plane), and the T subscript relates to the equatorial-belt strength anisotropy distribution for crack planes symmetrically distributed (centered) along a line (in this case the σ_x axis) (see also Fig. 3 for a reference frame). Figure 4 shows a schematic of Equations (29) and (30) in stress-strength space.

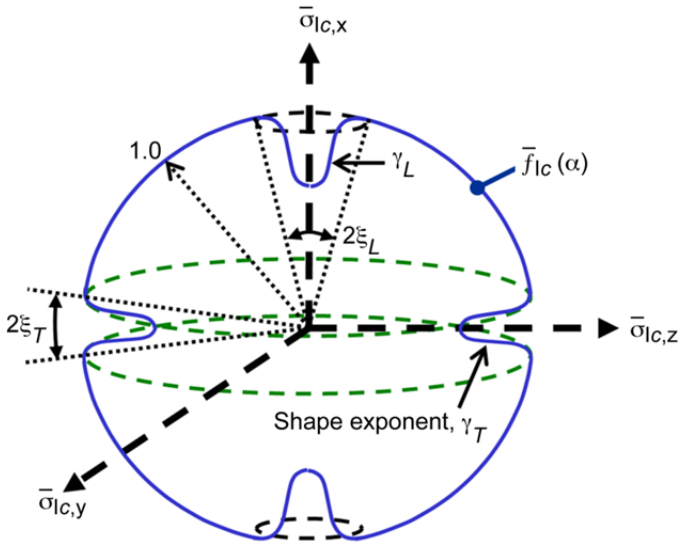

Figure 4.—Schematic of Equations (29) and (30) in normalized strength space. Equation (29) correlates to the polar-cap distribution, and Equation (30) correlates to the equatorial-belt distribution, as shown in Figure 3. Here, ξ_L, ξ_T, γ_L, and γ_T are constants in the critical mode I stress intensity anisotropy function representing longitudinal and transverse distributions; $\bar{f}_{Ic}(\alpha)$ is the normalized anisotropy function of the critical mode I stress-intensity factor, K_{Ic}, or critical mode I strength, σ_{Ic}, as a function of angle α; and $\bar{\sigma}_{Ic,x}$, $\bar{\sigma}_{Ic,y}$, and $\bar{\sigma}_{Ic,z}$ are the normalized (by $\sigma_{Ic,max}$) orthogonal critical strength components.

2.3.3 Generalized Unit-Sphere Failure Probability Formulation for Transverse Isotropy

Equations (26), (27), (29), and (30) are arbitrary functions chosen for their flexibility to fit to data. Other functions could be easily substituted. For an isotropic distribution of the orientation of the flaws, $\wp(\alpha, \beta)$ is $1/2\pi$, which is consistent with Equation (21). Although not detailed herein, the Weibull modulus can also be made anisotropic, varying with angles α and β, by using, for example, the normalizing Equations (29) and (30) to modify m (dividing m by $\bar{f}_{Ic}(\alpha)$). Therefore, in its most generalized form for transverse isotropy (considering flaw and critical strength orientation anisotropy), failure probability can be expressed as

$$P_{fV} = 1 - \exp\left[- \int_V \int_0^{2\pi} \int_0^{\pi/2} \int_0^{\sigma_{1eq,\max}} \frac{d\eta_V\left(\sigma_{1eqc}\right)}{d\sigma_{1eqc}} \wp(\alpha,\beta) \sin\alpha \; d\sigma_{1eqc} \; d\alpha \; d\beta \, dV \right] \tag{31}$$

and, if a power law is assumed for the crack-density function,

$$\eta_V\left(\sigma_{1eq}\right) = k_{BV}(\alpha,\beta)\left(\frac{\sigma_{1eq}(x,y,z,\alpha,\beta)}{\bar{f}_{Ic}(\alpha,\beta)} \right)^{m_V(\alpha,\beta)} = \bar{k}_{BV}\left(\frac{\sigma_{1eq}(x,y,z,\alpha,\beta)}{\bar{f}_{Ic}(\alpha,\beta)\sigma_{oV}(\alpha,\beta)} \right)^{m_V(\alpha,\beta)} \tag{32}$$

where critical strength or K_{Ic} orientation anisotropy is accounted for with the addition of the term $\bar{f}_{Ic}$. The Weibull modulus m_V is allowed to be a function of α and β. Note that the Weibull scale parameter σ_{oV} is used in the crack-density formulation and that it is also allowed to be a function of α and β, but that it is assumed to be constant with spatial location x, y, z. Equation (31) can then be more simply expressed as

$$P_{fV} = 1 - \exp\left[- \int_V \int_0^{2\pi} \int_0^{\pi/2} \bar{k}_{BV}\left(\frac{\sigma_{1eq}(x,y,z,\alpha,\beta)}{\bar{f}_{Ic}(\alpha,\beta)\sigma_{oV}(\alpha,\beta)} \right)^{m_V(\alpha,\beta)} \wp(\alpha,\beta) \sin\alpha \; d\alpha \; d\beta \, dV \right] \tag{33}$$

2.4 Orientation Distribution of Critical Flaws Under Multiaxial Load

The unique feature of the unit-sphere methodology is the assumption that the flaws that are inherently present in a brittle material will drive the failure response and that these flaws are microcracks with an assumed orientation and geometry. In this manner, the stochastic strength response of the material can be predicted for an arbitrary multiaxial stress state. An interesting consequence of this methodology is that the orientation of the critical flaws (the failure-initiating flaws) relative to the applied stresses can be predicted as a probabilistic distribution. The PDF of the orientation of the critical fracture-causing flaws can be obtained from Equations (10), (13), (16), and (19) for an isotropic strength material; from Equations (22), (23), and (24) for flaw orientation anisotropy; and from Equation (28) for critical strength (fracture-toughness) orientation anisotropy. How this is obtained is described subsequently for transverse isotropy.

For a given flaw (a flaw that is assumed to exist at some orientation α and β) and considering all possible flaw orientations, the likelihood must be 1 (in other words, 100-percent certainty) that the flaw exists at some orientation α and β. In other words,

$$\text{Probability that a flaw exists at some } \alpha \text{ and } \beta = 1 = \bar{c}_{\angle}\left[\int_0^{2\pi} \int_0^{\pi/2} \zeta(\alpha,\beta) \sin\alpha \; d\alpha \; d\beta \right] \tag{34}$$

where $\bar{c}_{\angle}$ is a normalizing constant and the function $\zeta(\alpha, \beta)$ describes the degree of anisotropy of flaw orientation at angular coordinates α and β (where the normal direction to the flaw plane is given by angles α

and β). The function ζ was defined in Equations (26) and (27) for a transversely isotropic strength response (which is expressed only as a function of angle α). Therefore, in Equation (34) $\bar{c}_{\angle}$ must equal

$$\bar{c}_{\angle} = \frac{1}{\int_0^{2\pi}\int_0^{\pi/2} \zeta(\alpha,\beta)\sin\alpha \, d\alpha \, d\beta} \tag{35}$$

The probability that the flaw is oriented in the range between α and (α + dα) and between β and (β + dβ) is given by $\wp(\alpha, \beta)\, d\alpha\, d\beta$ in Equation (24). In this case, an infinitesimal area element $dA = d\alpha\, d\beta$ on the unit sphere is represented as shown in Figure 5. In contrast to Figure 1(b), the sine term is not used here to describe d*A*. Figure 1(b) maintains a convention previously used in other references such as Nemeth et al. (2003, 2005). The sine term is only necessary when integration over the whole unit sphere is required. In order to determine the PDF of the orientation of the critical flaws, d*A* must be kept constant versus angular coordinates α and β. If $dA = \sin\alpha\, d\beta\, d\alpha$ were used, the nonsensical condition would be obtained that the probability of a flaw being oriented at α = 0 would always be zero regardless of the stress state and the magnitude of the stress.

Equation (24) is the PDF of the degree of anisotropy of the flaw orientation. Integration of the numerator of Equation (24) over the entire unit sphere for $dA = \sin\alpha\, d\beta\, d\alpha$ yields a value identical to the denominator, satisfying the condition for a PDF that integration over all possible values must equal 1 (for the cumulative distribution function).

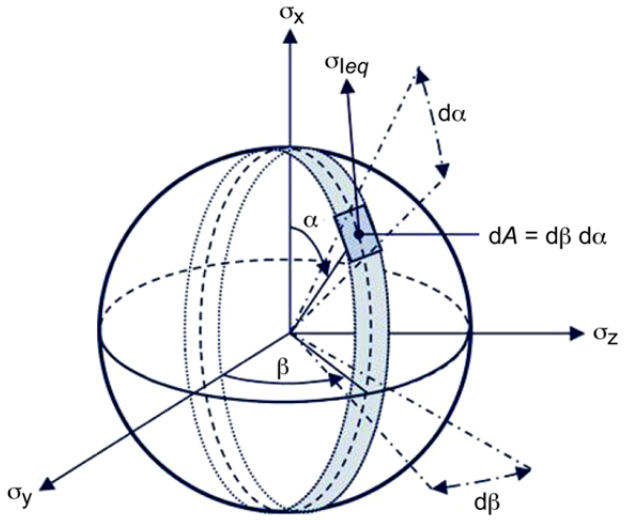

Figure 5.—Infinitesimal area element, d*A*, on the unit sphere. In this case, $dA = d\alpha\, d\beta$ for a given α and β orientation of the normal to the flaw plane, where σ_{leq} is the effective stress.

The probability that a flaw of strength σ_{leqc} or less that is within the incremental volume element Δ*V*, where $\sigma_{leq}(\Sigma, \alpha, \beta) \geq \sigma_{leqc}$, and that is oriented between α and (α + dα) and between β and (β + dβ), will fail is (see also Eq. (3))

$$P_{fV}(\Sigma,\alpha,\beta,\Delta V) = \wp(\alpha,\beta)\ \mathrm{d}\alpha\,\mathrm{d}\beta\ \eta_V(\alpha,\beta)\ \Delta V = \frac{\left[\zeta(\alpha,\beta)\ \mathrm{d}\alpha\ \mathrm{d}\beta\right]\ \eta_V(\alpha,\beta)\ \Delta V}{\int_0^{2\pi}\int_0^{\pi/2}\ \zeta(\alpha,\beta)\sin\alpha\ \mathrm{d}\alpha\ \mathrm{d}\beta} \tag{36}$$

where $P_{fV}(\Sigma, \alpha, \beta, \Delta V)$ is expressed for a constant infinitesimal area element $\mathrm{d}A = \mathrm{d}\alpha\,\mathrm{d}\beta$ on the unit sphere as shown in Figure 5 regardless of the specific values of angles α and β.

The failure probability for the whole unit sphere for incremental volume element ΔV is

$$P_{fV}(\Sigma,\Delta V) = \frac{\left[\int_0^{2\pi}\int_0^{\pi/2}\zeta(\alpha,\beta)\,\eta_V(\alpha,\beta)\sin\alpha\,\mathrm{d}\alpha\,\mathrm{d}\beta\right]\Delta V}{\int_0^{2\pi}\int_0^{\pi/2}\ \zeta(\alpha,\beta)\sin\alpha\ \mathrm{d}\alpha\ \mathrm{d}\beta} \tag{37}$$

Reexpressing Equation (37) using the crack-density function of Equation (32), using Equation (35) for $\bar{c}_{\angle}$, and considering critical strength or K_{Ic} orientation anisotropy yields

$$P_{fV}(\Sigma,\Delta V) = \left[\int_0^{2\pi}\int_0^{\pi/2}\bar{c}_{\angle}\ \zeta(\alpha,\beta)\ \bar{k}_{BV}\left(\frac{\sigma_{\mathrm{I}eq}(\alpha,\beta)}{\bar{f}_{\mathrm{I}c}(\alpha,\beta)\ \sigma_{oV}(\alpha,\beta)}\right)^{m_V(\alpha,\beta)}\ \sin\alpha\,\mathrm{d}\alpha\,\mathrm{d}\beta\right]\Delta V \tag{38}$$

The probability that the critical flaw (the failure-initiating flaw) is oriented in the range between α and (α + dα) and between β and (β + dβ) that is under a given stress state Σ is found by dividing $P_{fV}(\Sigma, \alpha, \beta, \Delta V)$ in Equation (36) by $P_{fV}(\Sigma, \Delta V)$ in Equation (37):

$$\wp_c(\Sigma,\alpha,\beta) = \frac{\left[\zeta(\alpha,\beta)\,\mathrm{d}\alpha\ \mathrm{d}\beta\right]\eta_V(\alpha,\beta)}{\int_0^{2\pi}\int_0^{\pi/2}\zeta(\alpha,\beta)\,\eta_V(\alpha,\beta)\sin\alpha\,\mathrm{d}\alpha\,\mathrm{d}\beta} \tag{39}$$

The numerator in Equation (39) refers to an infinitesimal area element $\mathrm{d}A = \mathrm{d}\alpha\,\mathrm{d}\beta$ on the unit sphere as shown in Figure 5. The PDF of Equation (39) is therefore

$$\wp_{\angle}(\Sigma,\alpha,\beta) = \frac{\zeta(\alpha,\beta)\,\eta_V(\alpha,\beta)}{\int_0^{2\pi}\int_0^{\pi/2}\zeta(\alpha,\beta)\,\eta_V(\alpha,\beta)\sin\alpha\,\mathrm{d}\alpha\,\mathrm{d}\beta} \tag{40}$$

Integration of the numerator of Equation (40) over the entire unit sphere for $\mathrm{d}A = \sin\alpha\,\mathrm{d}\beta\,\mathrm{d}\alpha$ yields a value identical to the denominator, satisfying the condition for a PDF that integration over all possible values must equal 1 (for the cumulative distribution function). Substituting Equation (32) into Equation (40) yields

$$\wp_{\angle}(\Sigma,\alpha,\beta) = \frac{\zeta(\alpha,\beta)\ \ k_{BV}\left(\dfrac{\sigma_{\mathrm{I}eq}(\alpha,\beta)}{\bar{f}_{\mathrm{I}c}(\alpha,\beta)}\right)^{m_V(\alpha,\beta)}}{\int_0^{2\pi}\int_0^{\pi/2}\zeta(\alpha,\beta)\,k_{BV}\left(\dfrac{\sigma_{\mathrm{I}eq}(\alpha,\beta)}{\bar{f}_{\mathrm{I}c}(\alpha,\beta)}\right)^{m_V(\alpha,\beta)}\ \sin\alpha\,\mathrm{d}\alpha\,\mathrm{d}\beta} \tag{41}$$

However, for computational convenience, the effective stress σ_{1eq} should be normalized by the scale parameter σ_{oV} and the normalized Batdorf crack-density coefficient $\bar{k}_{BV}$. If it is assumed that σ_{oV} and m_V are independent of angles α and β,

$$\wp_{\angle}(\Sigma,\alpha,\beta) = \frac{\zeta(\alpha,\beta)\left(\dfrac{\sigma_{1eq}(\alpha,\beta)}{\bar{f}_{1c}(\alpha,\beta)\,\sigma_{oV}}\right)^{m_V}}{\displaystyle\int_0^{2\pi}\int_0^{\pi/2}\zeta(\alpha,\beta)\left(\frac{\sigma_{1eq}(\alpha,\beta)}{\bar{f}_{1c}(\alpha,\beta)\,\sigma_{oV}}\right)^{m_V}\sin\alpha\,d\alpha\,d\beta} \tag{42}$$

Equation (42) describes the PDF of the orientation of critical flaw normals from the applied stress state Σ. However, these equations only describe the probability of the orientation of the critical flaw, they do not describe the angle of subsequent crack propagation. For noncoplanar crack growth, the action of a simultaneous normal stress and a shear stress will cause the crack to propagate at an angle θ relative to the plane of the initial flaw or microcrack. The anisotropy of material properties can also affect the angle of propagation. This direction of growth will be the direction of cracking that would be observed in rupture experiments (or loading experiments to the point of reaching the proportional limit or some level of damage threshold). Actually observing the orientation of the critical flaw would be difficult. This report does not consider the topic of crack propagation in an anisotropic medium. Nonetheless, the methodology described in this report provides a mechanistic-based framework for which to describe orientation distribution for critical flaws.

3.0 Examples

3.1 Isotropic Material Critical Flaw Orientation Probability Density Distribution

Fortran was used to implement a gaussian quadrature numerical integration algorithm to compute the generalized probability of failure equation (Eq. (33)) and the PDF equation for the orientation of critical flaws (Eq. (42)). This algorithm procedure is the same as that described in Nemeth et al. (2005), except that the integration is performed sequentially over smaller discrete sectors of the unit sphere. The numerical output from the Fortran code was used with MATLAB (MathWorks) software to plot the PDD (which herein are the results from the PDF) over the unit sphere. Values for parameters related to critical strength anisotropy (Eqs. (29) and (30)) are sensitive to the number of sampling points (number of gauss points, NGP) used in the numerical integration. When a greater number of points are used, the numerical solution asymptotically approaches a single value. In the following plots of the unit sphere (Figs. 6 to 11), a smaller number of sampling points was used (NGP = 5) for computational efficiency. This somewhat affected the numerical values of parameter r_T but not the trends seen in the figures. Results for Table I and Figures 12 to 15 were generated for NGP = 30, which represents fully converged solutions.

TABLE I.—VALUES OF PARAMETER r_T (SEE EQ. (30)) FOR VARIOUS STRENGTH RATIOS OF THE STRONGEST TO WEAKEST MATERIAL STRENGTH DIRECTIONS UNDER UNIAXIAL TENSILE LOADING

Strength ratio	Parameter r_T			
	Parameter, ξ_T, deg			
	10		90	
	Shetty shear sensitivity, $\overline{C}$			
	1.1236	100.0	1.1236	100.0
1.25	1.57	1.47	1.39	1.29
1.5	1.95	1.83	1.82	1.59
2.0	2.68	2.52	2.83	2.21
3.0	4.15	3.91	5.44	3.51
4.0	5.64	5.32	8.83	4.87
6.0	8.68	8.18	17.90	7.68
8.0	11.77	11.10	30.01	10.59
10.0	14.91	14.06	45.18	13.58

Figure 6 shows an example of the PDD from Equation (42) of critical flaws on the unit sphere for an isotropic material with a 100-MPa uniaxial tensile load applied in various directions. Figures 6(a), (b), and (c) show results for a uniaxial load applied in the x, y, and z material axes, respectively. The plots show the direction normal to the flaw plane as depicted schematically in Figure 1. As would be expected, the "spot" is centered on the direction of applied load, with the highest probability of orientation perpendicular to the applied load (dark red (center of "bullseye" shapes) indicates the highest probability and blue (background color) indicates the lowest probability). Figures 6(a), (b), and (c) are shown to demonstrate that the numerical algorithm and plotting software correctly reproduce the same results regardless of the direction of the applied load. Figure 6(d) shows the PDD numerical distribution versus angles α and β for an applied uniaxial tensile load in the z direction. Figure 6 is generated for an incremental unit volume with a load level corresponding to $P_{fV} = 0.6321$ (for $\sigma_{oV} = 100$ MPa·m$^{1/10}$), $m_V = 10$, and $\overline{C} = 1.5$ for mild shear sensitivity (using Eq. (11)). All subsequent plots were generated for $P_{fV} = 0.6321$ and $\sigma_{oV} = 100$ MPa·m$^{1/10}$.

The size (angular extent) of the "spot" (or distribution) shown in Figure 6 is a function of m_V and $\overline{C}$. This is demonstrated in Figure 7 for a uniaxial tensile load applied in the y direction. The plots show that the higher m_V is, the more localized (more confined or highly aligned) the "spot" with the applied load is (flaws are more perpendicular to the applied load) as shown in Figures 7(a), (c), and (e). The same is also true with $\overline{C}$, where for the shear-insensitive condition ($\overline{C} = 100.0$), the spot is more tightly distributed as shown in Figures 7(b), (d), and (f) and, as $\overline{C}$ gets smaller (shown as $\overline{C} = 1.5$ for mild shear sensitivity), the spot is less tightly distributed as shown in Figures 7(a), (c), and (e).

Figure 8 shows the effect of shear-sensitivity parameter $\overline{C}$ for an applied shear stress τ_{yz} for $m_V = 10$. Results for increasing shear sensitivity for $\overline{C} = 100.0$ (shear-insensitive), $\overline{C} = 1.5$ (mildly shear-sensitive), and 0.82 (highly shear-sensitive) are shown in Figures 8(a), (c), and (e), respectively. In Figures 8(a) and (b), only the normal tensile stress component contributes to failure, and the spot of highest probability is centered on $\alpha = 90°$ and $\beta = 45°$. In Figures 8(c) and (d), for the case of mild shear sensitivity, the spot of the highest probability bifurcates and the two spots are symmetrically offset at a small β angle from $\alpha = 90°$ and $\beta = 45°$. This indicates that the effect of shear sensitivity on the micro-crack alters the angle of most probable fracture for an applied shear stress. This is further shown in Figures 8(e) and (f) where a high shear sensitivity shows two distinctly different fracture planes, but their symmetry is oriented about $\alpha = 90°$ and $\beta = 45°$. An additional note about Figures 8(e) and (f) is that, when the normal stress on the flaw plane becomes compressive, the failure probability associated with that orientation for the tensile failure mode is set to zero in the numerical method; hence, there is some truncation that can be seen in the figure, where the color fringes drop out (left side of the left spot and right side of the right spot).

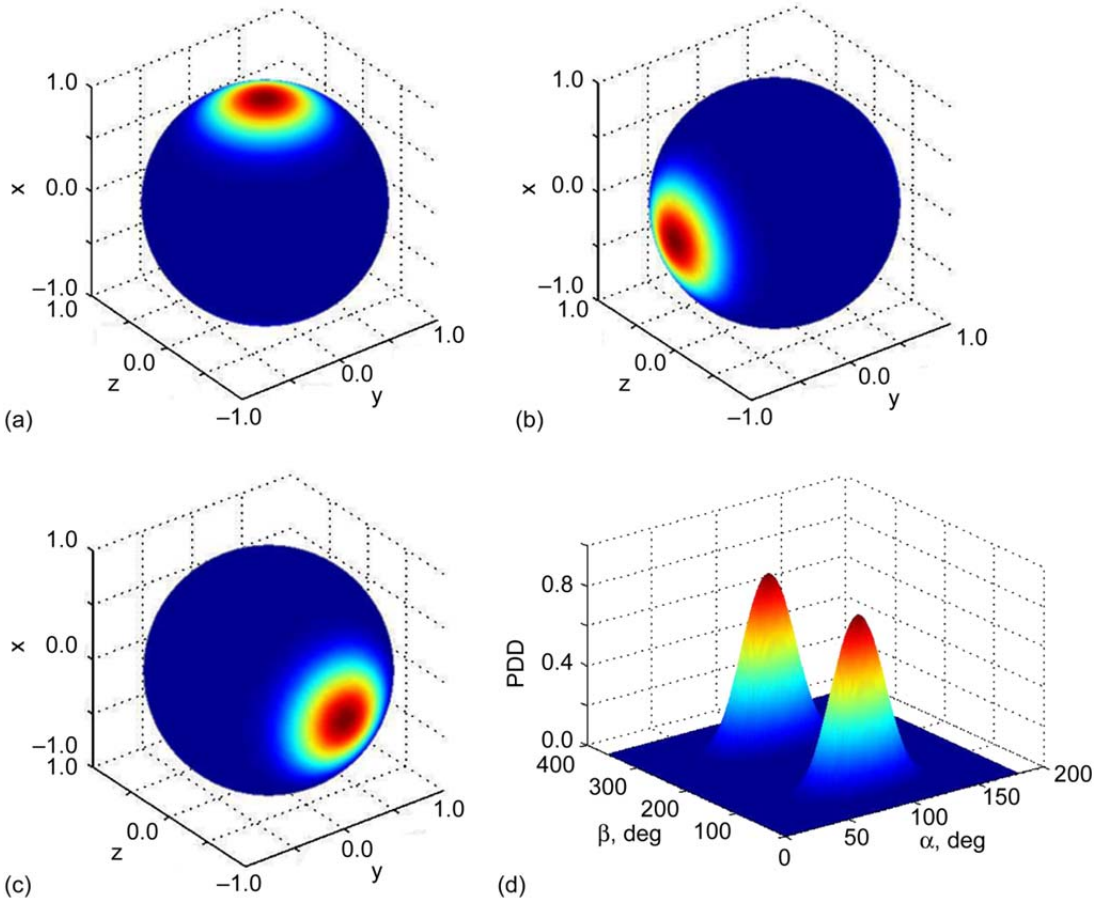

Figure 6.—Probability density distribution (PDD) plots of the orientation of critical flaws on the unit sphere for a 100-MPa uniaxial tensile load for an isotropic material. The center of the "spot" indicates the highest likelihood of orientation. This tests the consistency of calculated results for loading in various directions. Here the Weibull modulus, m_V = 10.0, and the Shetty shear sensitivity, $\overline{C}$ = 1.5. (a) Load in the x direction. (b) Load in the y direction. (c) Load in the z direction. (d) PDD in terms of magnitude normalized to radians for angles α and β of the load in the z direction.

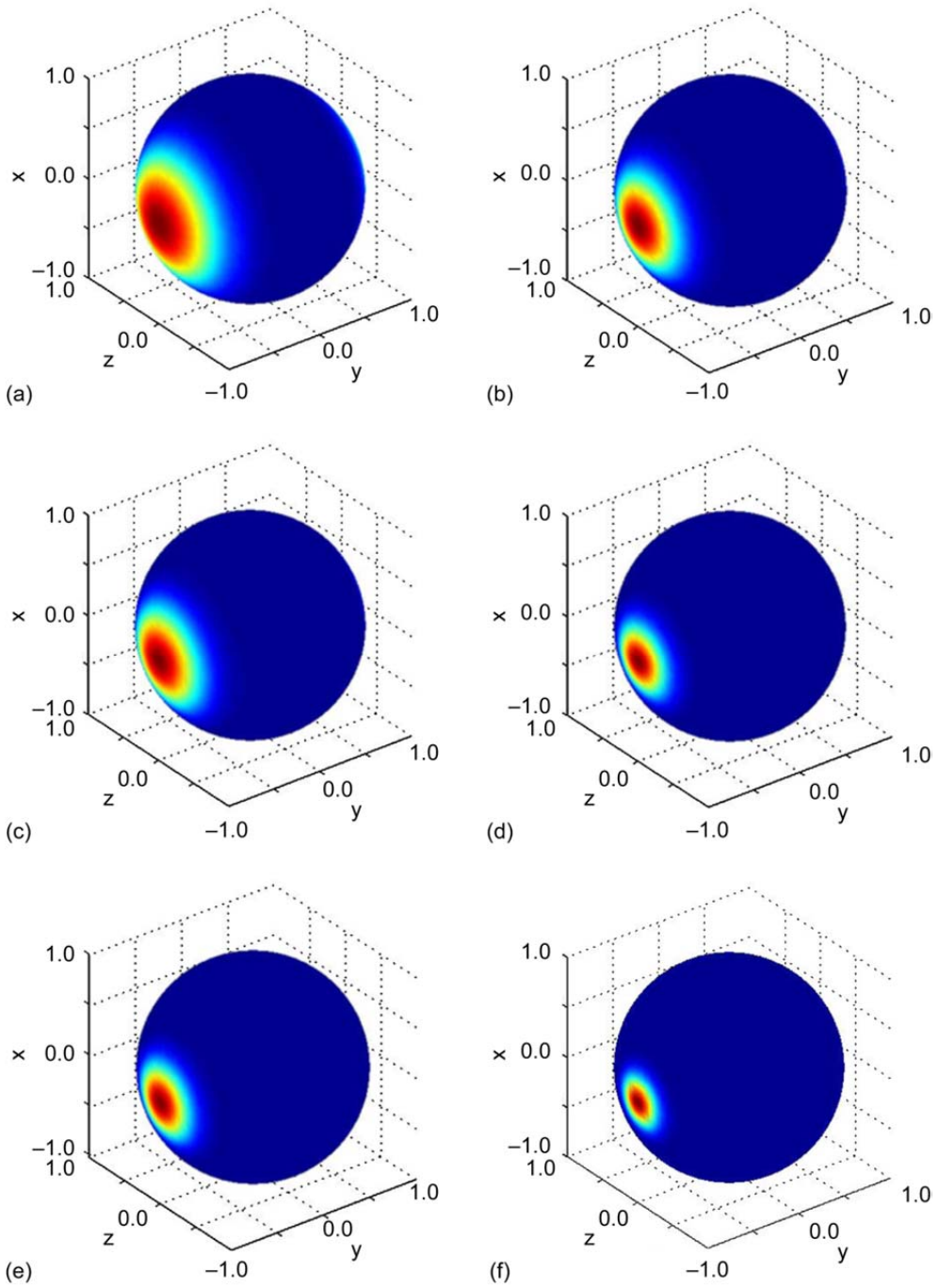

Figure 7.—Probability density distribution (PDD) plots of the orientation of critical flaws on the unit sphere for an isotropic material with a 100-MPa uniaxial tensile load applied in the y direction, showing the effect of Weibull modulus, m_V, and Shetty shear sensitivity, $\overline{C}$. (a) m_V = 5.0 and $\overline{C}$ = 1.5. (b) m_V = 5.0 and $\overline{C}$ = 100.0. (c) m_V = 10.0 and $\overline{C}$ = 1.5. (d) m_V = 10.0 and $\overline{C}$ = 100.0. (e) m_V = 20.0 and $\overline{C}$ = 1.5. (f) m_V = 20.0 and $\overline{C}$ = 100.0.

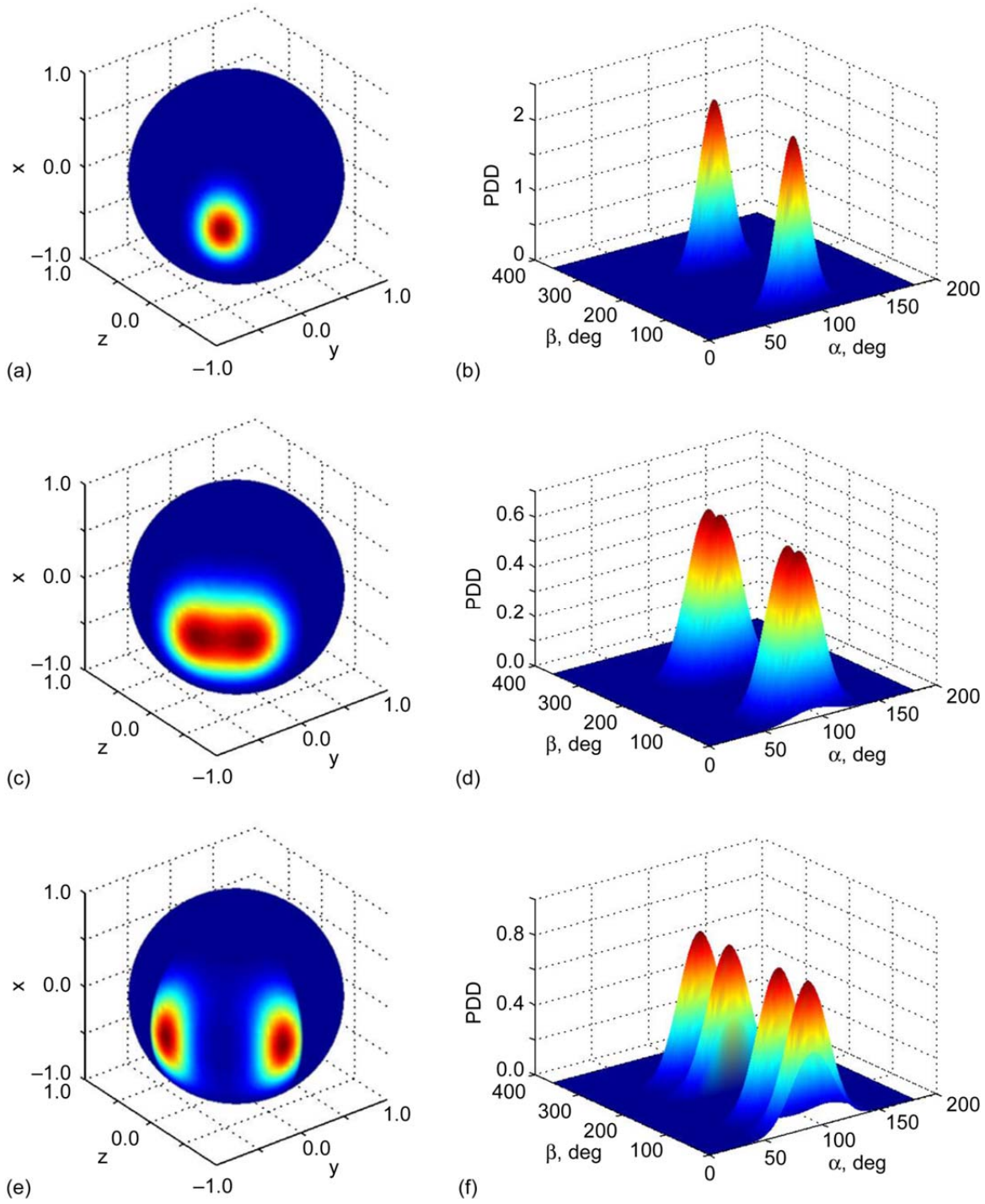

Figure 8.—Probability density distribution (PDD) plots of the orientation of critical flaws on the unit sphere for an isotropic material for a τ_{yz} = 100-MPa shear stress showing the effect of Shetty shear sensitivity, $\overline{C}$. (a) Weibull modulus, m_V = 10.0, and $\overline{C}$ = 100.0. (b) PDD in terms of magnitude for m_V = 10.0 and $\overline{C}$ = 100.0. (c) m_V = 10.0 and $\overline{C}$ = 1.5. (d) PDD in terms of magnitude for m_V = 10.0 and $\overline{C}$ = 1.5. (e) m_V = 10.0 and $\overline{C}$ = 0.82. (f) PDD in terms of magnitude for m_V = 10.0 and $\overline{C}$ = 0.82.

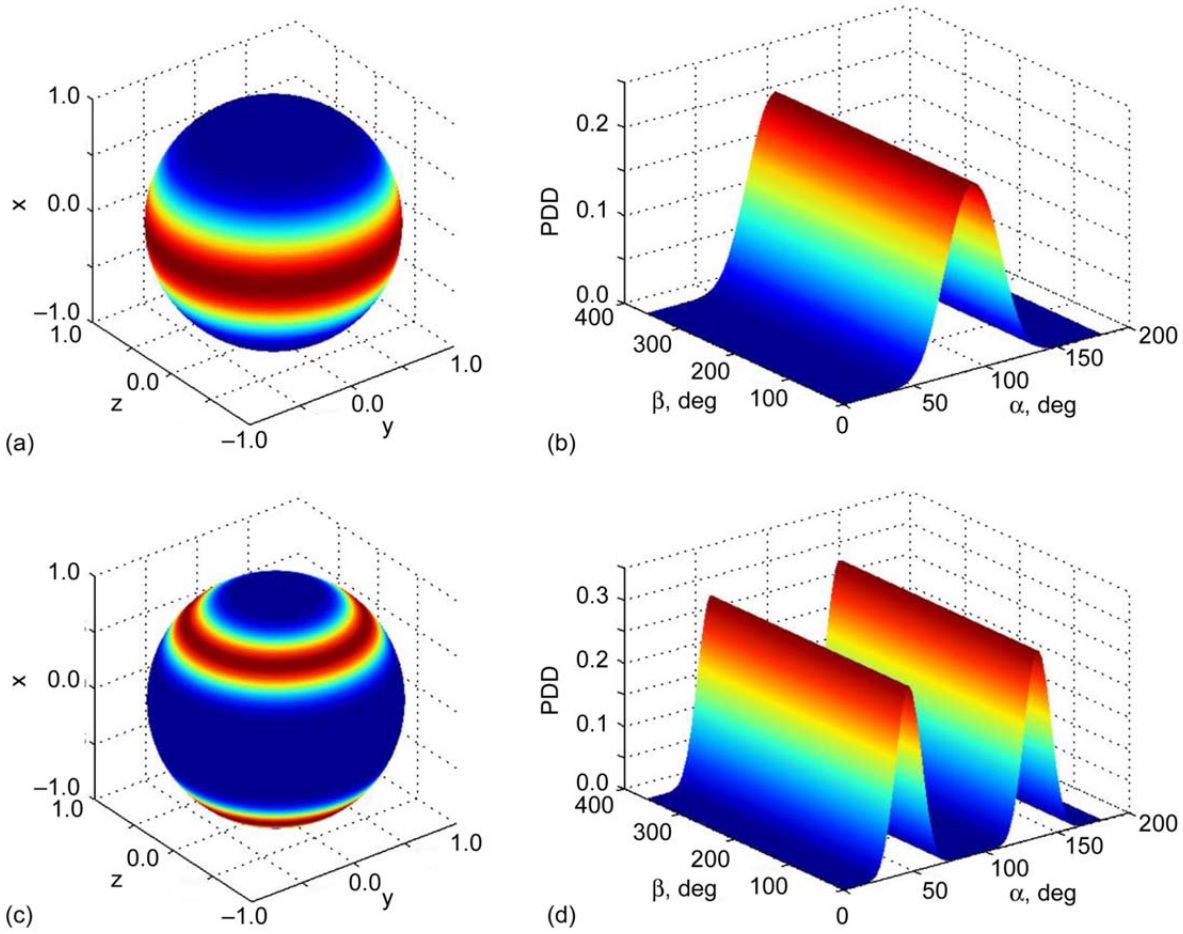

Figure 9.—Probability density distribution (PDD) plots of the orientation of critical flaws on the unit sphere for an isotropic material. (a) Equibiaxial tensile stress applied in the y and z directions, $\sigma_x = \sigma_y = 100$ MPa. (b) PDD in terms of magnitude of equibiaxial tensile stress. (c) Uniaxial compressive stress applied in the x direction, $\sigma_x = 500$ MPa. (d) PDD in terms of magnitude of uniaxial compressive stress. For the tensile failure mode, (a) and (b), the Weibull modulus, $m_V = 10.0$; $\sigma_{oV} = 100$ MPa (MPa•m$^{1/10}$), $\overline{C} = 1.5$ (Eq. (11)), $\nu = 0.22$; and the probability of failure of material volume, $P_{fV} = 0.6321$. For the compressive failure mode, (c) and (d), using Equation (12), $m_{\ell V} = 10$, the Weibull scale parameter for compression, $\sigma_{o\ell V} = 500$ MPa (MPa•m$^{1/10}$), and $P_{fV} = 0.6321$.

Figures 9(a) and (b) show an example of the unit sphere PDD for critical flaw orientation for an equibiaxial tensile stress state applied in the y and z axial directions ($\sigma_x = 0$; $\sigma_y = \sigma_z$). This plot was generated for a mildly shear sensitive material ($\overline{C} = 1.5$). The critical flaws have equal likelihood to be at any angle β in the y-z plane. Figures 9(c) and (d) show an example of the unit sphere PDD for the critical flaw orientation for a uniaxial compressive stress state for the compressive stress failure criterion using Equation (12). The critical flaw planes are oriented at 45° to the direction of applied loading—the x direction in this case.

3.2 Transversely Isotropic Material Critical Flaw Orientation Probability Density Distribution for Off-Axis Uniaxial Load

In this section, some examples of the critical flaw orientation PDD are shown for the critical strength anisotropy model of Section 2.3.2. Results for the flaw orientation anisotropy model of Section 2.3.1 are not shown (because plotted results would appear similar to that of the critical strength anisotropy model).

Figure 10 is an example of the unit sphere PDD for critical flaw orientation for a 2:1 transversely isotropic strength response. This model assumes critical strength anisotropy and uses Equation (30) to define the weaker directions of strength (the *T* distribution). In this case, a 50-MPa uniaxial tensile load (in the y material direction) is applied in the plane with the weakest material strength (the y-z plane) for $P_{fV} = 0.6321$. Figures 10(a) and (b) show the unit sphere PDD for the critical flaw orientation for a shear-insensitive ($\overline{C} = 100.0$) response, and Figures 10(c) and (d) show the results for a shear-sensitive response ($\overline{C} = 1.1236$, where $K_{Ic} = (K_{IIc}$ or $K_{IIIc})$ for $\nu = 0.22$), where the mode I strength of the flaw and the mode II (or mode III) of the flaw are equal. The strength response is for a material that has a more gradual critical strength transition from the strong to the weaker material strength direction ($\xi_T = \pi/2$ radians (90°) and $\gamma_T = 1$). As would be expected, a more oval or elliptical spot is observed in comparison to the isotropic material in Figure 6(b) because of the effect of the weaker y-z material plane.

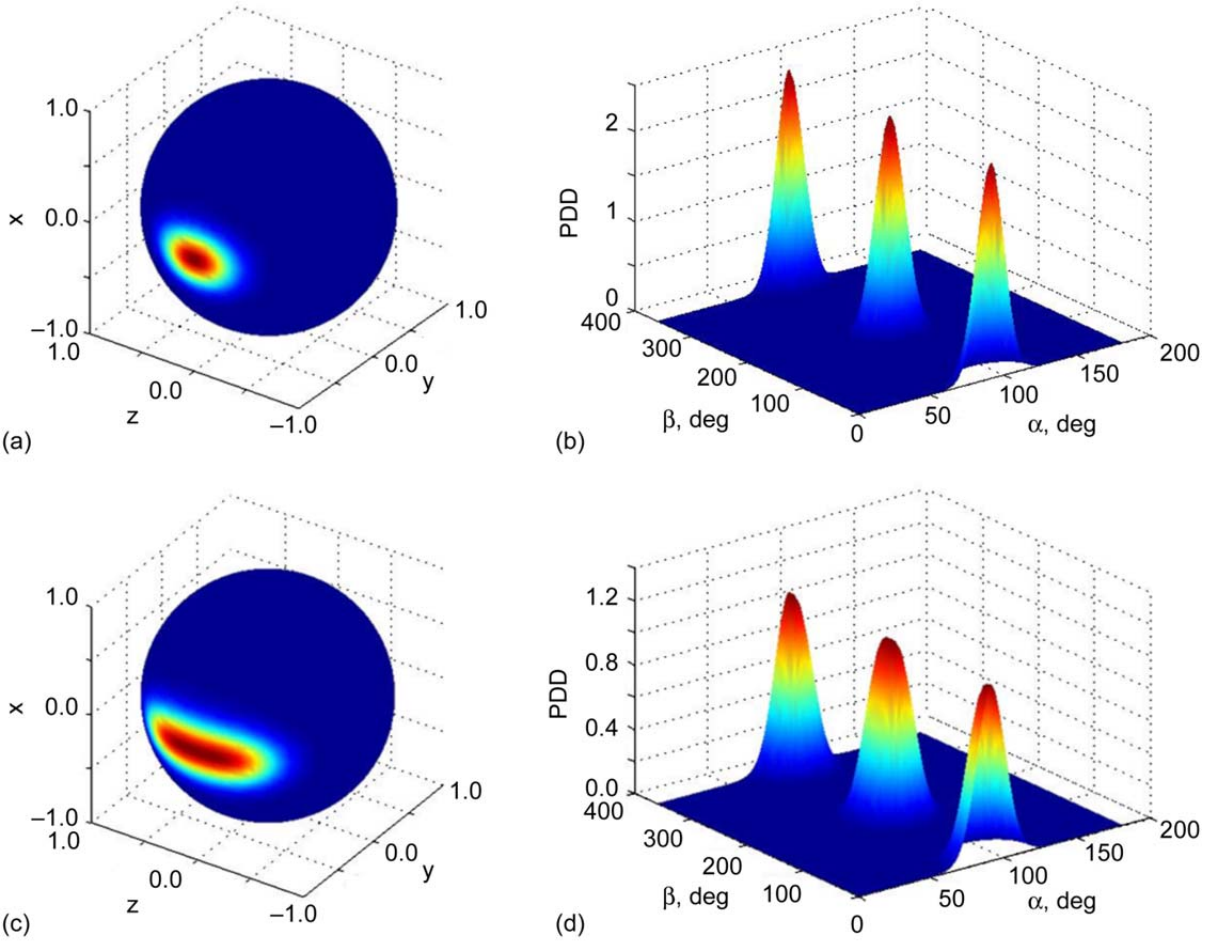

Figure 10.—Probability density distribution (PDD) plots of the orientation of critical flaws on the unit sphere for a shear-insensitive and shear-sensitive transversely isotropic material. This is for a 50-MPa uniaxial tensile load (in the y material direction) applied along the plane with the weakest material strength (the y-z plane). The strength ratio is 2:1, where critical mode I stress-intensity factor, K_{Ic}, anisotropy functions representing the transverse (equatorial-belt) distribution, $\xi_T = \pi/2$ radians (90°) and $\gamma_T = 1$. (a) Plot on unit sphere. (b) PDD in terms of magnitude for Shetty shear sensitivity, $\overline{C} = 100.0$ (shear-insensitive response), and parameter in K_{Ic} anisotropy function, $r_T = 2.21$. (c) Plot on unit sphere. (d) PDD in terms of magnitude for $\overline{C} = 1.1236$ (shear-sensitive response) and $\gamma_T = 2.83$. In both cases, the Weibull modulus, $m_V = 10$; the Weibull scale parameter, $\sigma_{oV} = 100$ MPa (MPa•m$^{1/10}$); and the probability of failure of material volume, $P_{fV} = 0.6321$.

Figure 11 is an example of the unit sphere PDD for the critical flaw orientation for a 3:1 transversely isotropic strength response for a uniaxial load offset 15° from the strong material direction ($\alpha = 15°$ and $\beta = 0°$). This model also uses Equation (30) to define the weaker directions of strength (the *T* distribution); however, the strength response is for a material that has a more abrupt critical strength transition from the strong to the weaker material strength direction ($\xi_T = 0.08727$ radians (5°), $\gamma_T = 0$, and $r_T = 3.56$). The load is a uniaxial tensile stress of 99.3 MPa for a $P_{fV} = 0.6321$. A relatively mild shear sensitivity ($\overline{C} = 1.4$) is assumed. The parameter $\gamma_T = 0$ corresponds to a uniform distribution over the equatorial belt where K_{Ic} is low relative to the rest of the unit sphere. This modeling scenario is arbitrary but may be considered to model the effect of a weak interface, such as between a fiber and matrix or within the matrix constituent, or possibly represent anisotropy in thin-film coatings where interfacial layers and anisotropically oriented microstructures are present. In addition to the PDD plot on the unit sphere (Fig. 11(a)), a numerical plot of the PDD versus angle of orientation of the flaw normal is shown (Fig. 11(b)). Contrasting the unit-sphere plots of Figures 10(a) and (c) with Figure 11(a), shows the effect of parameter ξ_T as a narrower strip (the smaller extent of angle α), where the critical flaw has a high likelihood of being centered on $\alpha = 90°$ and $\beta = 0°$. Figure 11 also shows the relative sensitivity of strength anisotropy with critical flaw angle. When the offset uniaxial load is only 15°, the probability that the critical flaw will be oriented about $\alpha = 90°$ and $\beta = 0°$ becomes significant. This leads to the question of how anisotropy affects the orientation of the most critical flaw that is predicted with this model.

Figures 12 to 15 were prepared to help investigate that question or to at least demonstrate that consequence with the unit-sphere model. These graphs plot the angle of highest probability (the orientation where the critical flaw PDD value is maximum) versus the angle of a uniaxial tensile load applied at some angle α. These figures were prepared using $m_V = 100$ MPa·m$^{1/10}$ and $P_{fV} = 0.6321$. The strongest material direction is at $\alpha = 0°$, and the weakest material direction is at $\alpha = 90°$. It bears

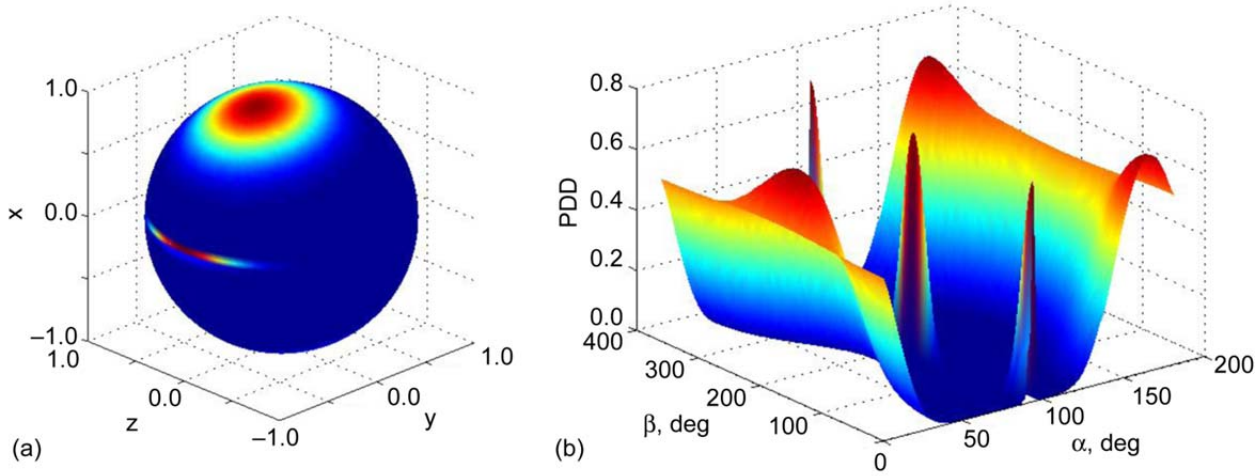

Figure 11.—Probability density distribution (PDD) of critical flaw normals for a 3:1 strength response for a transversely isotropic material. The load is a uniaxial tensile stress of 99.3 MPa applied at a 15° offset from the x axis ($\alpha = 15°$ and $\beta = 0°$). A relatively mild shear sensitivity ($\overline{C} = 1.4$) is assumed. (a) Plot on unit sphere. (b) PDD in terms of magnitude for Weibull modulus, $m_V = 10$; Weibull scale parameter, $\sigma_{oV} = 100$ MPa•m$^{1/10}$; Shetty shear sensitivity, $\overline{C} = 1.4$; Poisson's ratio, $\nu = 0.22$; parameters in the K_{Ic} anisotropy function representing the transverse (equatorial-belt) distribution: $\xi_T = 0.08727$ radians (5°), $\gamma_T = 0$, and $r_T = 3.563$; probability of failure of material volume, $P_{fV} = 0.6321$.

repeating that this is a prediction of the critically oriented flaw and not the direction of the subsequent crack propagation. The figures illustrate the effect of shear sensitivity $\overline{C}$, the abruptness of the critical strength transition from strong to weak response using parameter ξ_T, and the strong direction to weak direction strength ratio modeled with parameter r_T (see Table I). This line of inquiry was motivated by the observation that in CMCs the angle of microcracking for offset uniaxial tensile loads tends to be perpendicular to the direction of applied loading (e.g., Cady et al. (1995) and Lynch and Evans (1996)). However, this is not universally the case, as shown in Figure 16 for a 0°/90° CMC laminate with a 30°-offset loading. In that case, the matrix cracks tended to be misaligned 12° to 15° with the perpendicular to the loading direction and approximately aligned symmetrically 45° from either fiber axis.

Figure 16 shows that adjacent plies can influence the microcracking pattern. This suggests that it may be plausible to consider the influence of the laminate as a whole and to construct anisotropic unit-sphere matrix failure criteria appropriately. However, at the microscale level, CMC failure behavior involves more complicated mechanisms including fiber interface debonding and sliding resistances. Therefore, for a CMC, the anisotropic unit-sphere material failure criterion may prove useful at the macroscale of the composite material or alternatively at the microscale of the individual constituents involving the matrix with the fiber where multiscale modeling would be requisite. At the macroscopic scale, Figures 12 to 15 would be appropriate for a unidirectional laminate where all the fibers are aligned in the same direction. When the individual plies are not aligned with one another, Equations (29) and (30) would have to be suitably modified.

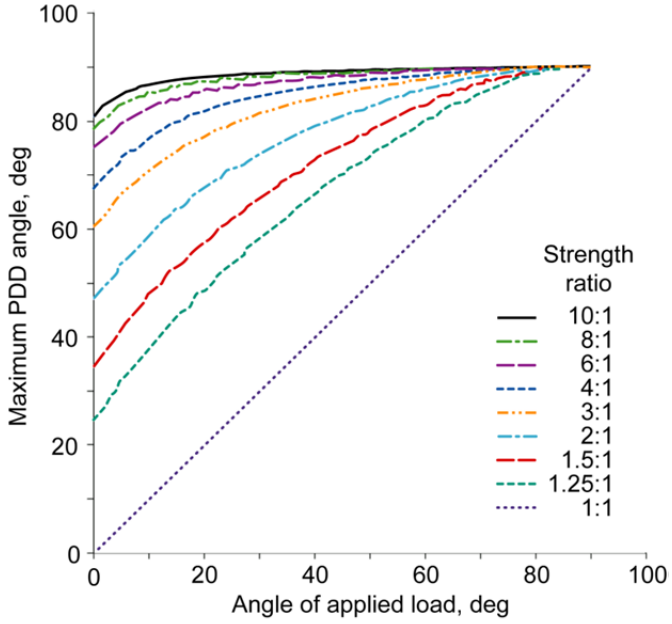

Figure 12.—Most probable orientation of the critical flaw relative to the offset angle of an applied uniaxial tensile load (at angle α on the unit sphere) for various anisotropic strength ratios. This example is for a mild critical strength transition (parameters in the critical mode I stress-intensity factor, K_{Ic}, anisotropy function representing the equatorial-belt distribution, $\xi_T = \pi/2$ radians (90°) and $\gamma_T = 1$) and high shear sensitivity $\overline{C} = 1.1236$ (mode I and mode II strength are equal). The strongest material direction is at $\alpha = 0°$, and the weakest material direction is at $\alpha = 90°$. PDD, probability density distribution.

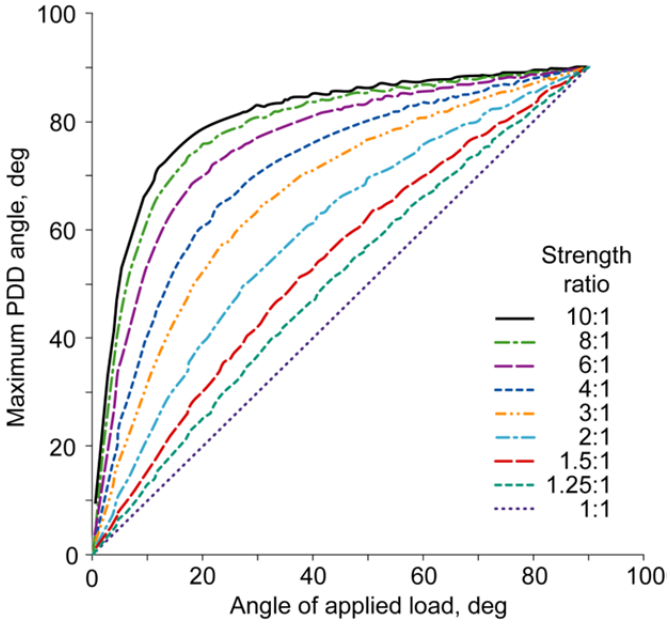

Figure 13.—Most probable orientation of the critical flaw relative to the offset angle of an applied uniaxial tensile load (at angle α on the unit sphere) for various anisotropic strength ratios. This example is for a mild critical strength transition (parameters in the critical mode I stress-intensity factor, K_{Ic}, anisotropy function representing the equatorial-belt distribution, $\xi_T = \pi/2$ radians (90°) and $\gamma_T = 1$) and shear insensitivity $\overline{C} = 100.0$. The strongest material direction is at $\alpha = 0°$, and the weakest material direction is at $\alpha = 90°$. PDD, probability density distribution.

Figure 12 shows the most probable orientation of the critical flaw relative to the offset angle for an applied uniaxial load for a mild mode I critical strength transition ($\xi_T = \pi/2$ radians (90°) and $\gamma_T = 1$) and high shear sensitivity $\overline{C} = 1.1236$ (where mode I and mode II strength are equal). Figure 13 shows the results for the case of shear insensitivity $\overline{C} = 100.0$ (with all other parameters the same). The mild critical strength transition is representative of materials such as graphite. Figures 12 and 13 indicate that the critical flaw angle deviates from the angle of offset load depending on the level of shear sensitivity and the degree of strength anisotropy. Figure 12 indicates that, when the uniaxial tensile load is applied in the strong material direction ($\alpha = 0°$), the critical flaw is already oriented at a significant angle of α away from the direction of applied load. This contrasts with Figure 13, where this angle is smaller—particularly for lower values of strength ratio, and tends to zero at $\alpha = 0°$. However, this angle of deviation increases rapidly as the angle of offset load increases from $\alpha = 0°$ for the higher levels of strength ratio. Figure 13 shows that the gradual critical strength transition from the strong material direction to the weak material direction strongly influences the orientation of the critical flaw for an offset load, and Figure 12 shows the additional influence of shear sensitivity combined with the mode I critical strength anisotropy.

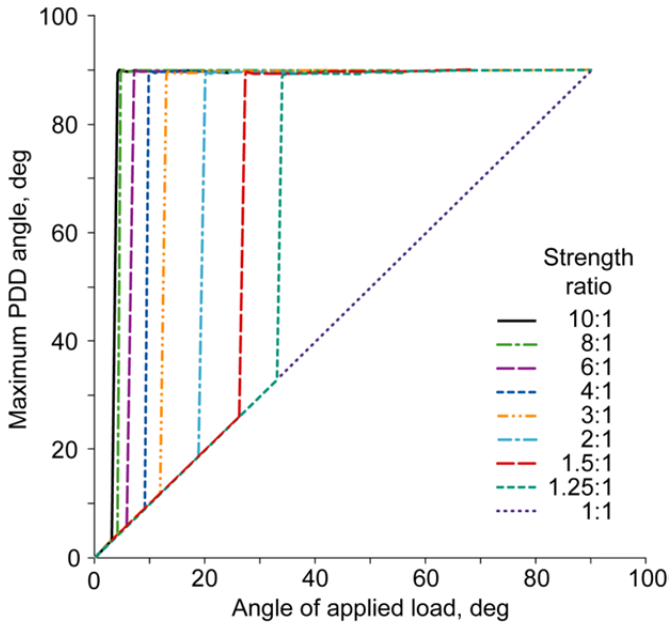

Figure 14.—Most probable orientation of the critical flaw relative to the offset angle of an applied uniaxial tensile load (at angle α on the unit sphere) for various anisotropic strength ratios. This example is for a strong critical strength transition (parameters in the critical mode I stress-intensity factor, K_{Ic}, anisotropy function representing the equatorial-belt distribution, ξ_T = 0.1745 radians (10°) and γ_T = 1) and high shear sensitivity $\overline{C}$ = 1.1236 (mode I and mode II strength are equal). The strongest material direction is at α = 0°, and the weakest material direction is at α = 90°. PDD, probability density distribution.

Figure 14 shows the most probable orientation of the critical flaw relative to the offset angle for an applied uniaxial load for an abrupt mode I critical strength transition (ξ_T = 0.1745 radians (10°) and γ_T = 1) and high shear sensitivity, $\overline{C}$ = 1.1236 (where mode I and mode II strength are equal). Figure 15 shows the results for the case of shear insensitivity $\overline{C}$ = 100.0 (with all other parameters the same). The abrupt mode I critical strength transition is intended to be representative of materials where an interface or inhomogeneity or abrupt shift in microstructure is present such as an interfacial boundary between the matrix and a fiber coating or the fiber itself, or between different deposition methods and/or materials on thin-film brittle coatings.

Figures 14 and 15 show the abrupt transition of the orientation of the critical flaw to the weak material direction α = 90° as the angle of the offset load increases. The abruptness of this transition can also be seen in Figure 11, where the offset angle was chosen near to where this transition occurs. Both figures indicate expected isotropic behavior prior to this transition where the most probable angle of the critical flaw is coincident with the angle of the applied loading (as also seen in Fig. 6 for the different directions of applied loading). In Figure 14, the shear sensitivity shifts the angle of where this transition occurs to smaller values of α in comparison to the shear insensitive condition of Figure 15. As the ratio of the strength anisotropy increases, it also shifts this transition to progressively smaller values of α.

A comparison of Figures 12 and 13 with Figures 14 and 15 shows the effect of parameter ξ_T on the most probable angle of the critical flaw. Even for a milder transition of the mode I critical strength ($\xi_T = \pi/2$ radians (90°)), the most probable orientation for the critical flaw trends toward $\alpha = 90°$ as the strength ratio increases. Overall, Figures 12 to 15 show the strong trend that the most probable orientation for the critical flaw is to shift toward the weaker material direction ($\alpha = 90°$) as the strength anisotropy ratio increases.

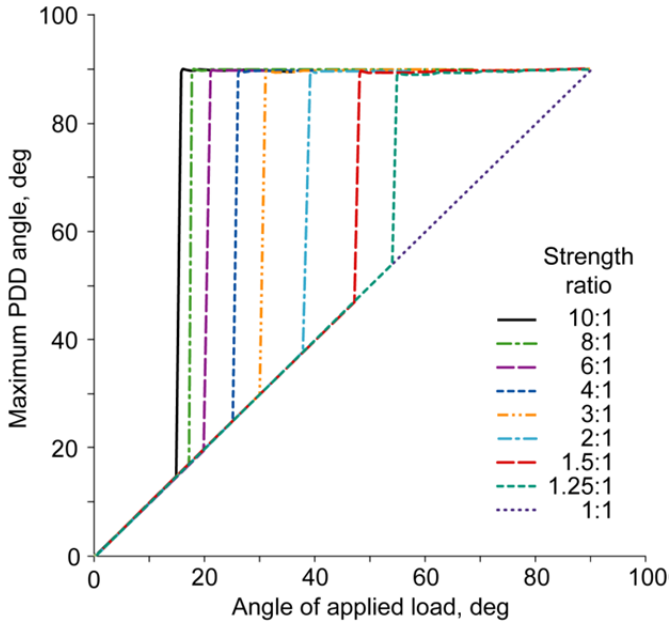

Figure 15.—Most probable orientation of the critical flaw relative to the offset angle of an applied uniaxial tensile load (at angle α on the unit sphere) for various anisotropic strength ratios. This example is for a strong critical strength transition (parameters in the critical mode I stress-intensity factor, K_{Ic}, anisotropy function representing the equatorial-belt distribution, $\xi_T = 0.1745$ radians (10°) and $\gamma_T = 1$) and shear insensitivity $\overline{C} = 100.0$. The strongest material direction is at $\alpha = 0°$, and the weakest material direction is at $\alpha = 90°$. PDD, probability density distribution.

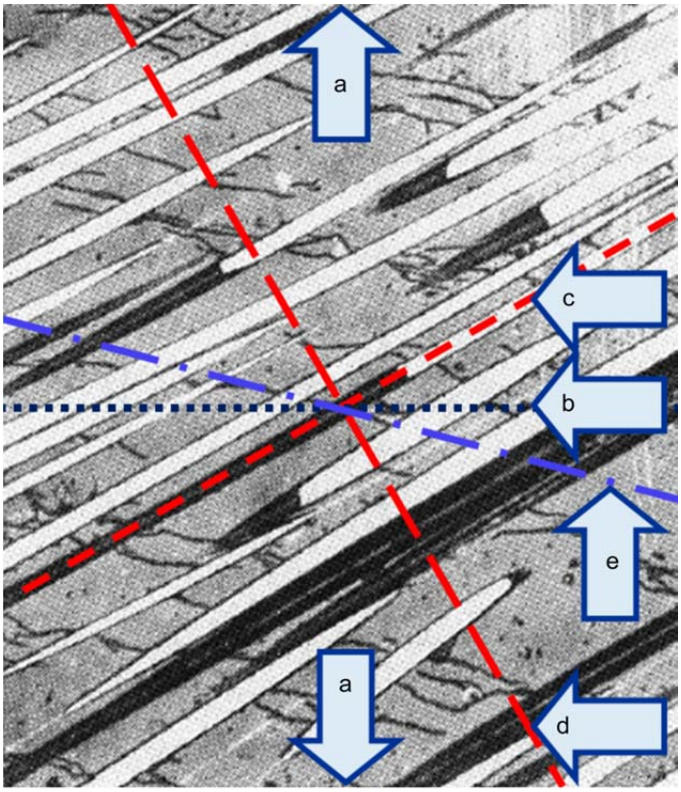

Figure 16.—Matrix cracking pattern from 30° off-axis loading of a 0°/90° ceramic matrix composite laminate from Lynch and Evans (1996). Matrix cracks appear to be 12° to 15° misaligned with the perpendicular to the loading direction, where a is the direction of loading, b is perpendicular to the loading direction, c is the fiber axis of the exposed ply, d is the fiber axis of the underlying ply, and e is 45° to either fiber axis.

4.0 Summary and Conclusions

A generalized equation was developed to describe the probability density function for the distribution of critical flaws from the Batdorf unit-sphere model for multiaxial loading. This formulation is for isotropic and anisotropic (transversely isotropic) brittle materials. The scenarios considered for anisotropic strength response were for (1) flaw orientation anisotropy, whereby a preexisting microcrack has a higher likelihood of being oriented in one direction than another direction, and (2) critical strength or fracture toughness anisotropy, where the level of critical strength or fracture toughness for mode I crack propagation changes with regard to the orientation of the microstructure.

A numerical algorithm was developed, and the results were plotted in MATLAB (MathWorks) for the unit-sphere probability density distribution (PDD) for various multiaxial stress states for an isotropic material. The results demonstrated that the PDD depends on the stress state, shear sensitivity of the flaws, and the Weibull modulus. Lower Weibull modulus and higher shear sensitivity meant higher dispersion of the distribution of critical flaws for a uniaxial stress state. For a pure shear stress state, when the shear sensitivity of the flaws increased, the orientation distribution of the critical flaws bifurcated into the two preferred angles of highest probability. This report also showed PDD results for an equibiaxial stress state and a uniaxial compressive stress state.

For transversely isotropic strength response, an example was shown of the PDD for a uniaxial tensile load applied at an angle offset from the strongest material direction. The angle of highest probability for the critical flaw also was investigated versus the offset loading angle for various anisotropic strength ratios and abruptness of the strength dropoff for the mode I critical strength anisotropy model. These results indicate that when there was an abrupt dropoff in mode I critical strength, there was also an abrupt transition of the angle of the critical flaw versus the offset angle of the applied uniaxial load such that the critical flaw angle became normal to the weakest material direction. These results also were sensitive to the level of shear sensitivity. Even for a more gradual dropoff in mode I critical strength (versus orientation) the most probable critical flaw angle tended to align with the weakest material direction as the loading offset angle increased and as the anisotropic strength ratio increased. Overall, there was a strong tendency for the most probable angle of the critical flaw to quickly align with the weakest material direction as the offset loading angle increased and as anisotropic strength ratio increased, even with a more gradual transition of mode I critical strength anisotropy versus orientation on the unit sphere.

If one knows the orientation distribution of critical flaws (and the subsequent direction of crack propagation), the anisotropic stiffness degradation (the anisotropic elastic constants associated with the damaged material) can be determined. The author anticipates that this will be helpful for a follow-on phase of this effort, not described here, of enabling the unit-sphere failure criterion methodology to work with NASA's micromechanics analysis code/generalized method of cells (MAC/GMC, Bednarcyk and Arnold (2002)). This incorporation will allow the full exercise of the unit-sphere methodology, including incremental time/load steps and fatigue analysis (as described in Nemeth, Noel N.; Gyekenyesi, J.P.; and Jadaan, Osama M. (2005): Lifetime Reliability Prediction of Ceramic Structures Under Transient Thermomechanical Loads. NASA/TP—2005-212505. http://ntrs.nasa.gov/), to predict the durability (strength and lifetime) of composite laminates and woven composite structures.

The development of the anisotropic unit-sphere methodology was an attempt to provide an improved mechanistic basis to the problem of predicting composite strength under multiaxial loading in comparison to the phenomenologically based polynomial formulations such as Tsai-Wu, Tsai-Hill, and Hashin. The interesting consequence of this work was that the PDD on the unit sphere of the orientation of critical-strength-controlling flaws could also be predicted. That formulation and the demonstration of that capability was the subject of this report.

This technology has general relevance to the anisotropic strength response of brittle materials. This may include thin-film coatings such as environmental barrier coatings where tensile stresses play a significant role in coating integrity. The need for additional enhancements is anticipated, such as the determination of the angle of noncoplanar crack growth and the development of the anisotropic stiffness matrix for a damaged material.

Appendix—Symbols

A	area
dA	infinitesimal area on the surface of a unit radius sphere
a	crack length or crack radius
a_c	critical crack length or crack radius
$\overline{C}$	Shetty shear-sensitivity coefficient
c	constant
$\overline{c}_{\angle}$	normalizing constant
$f(x)$	discrete density function of random variable X where $P(X = x)$
$\overline{f}_{\mathrm{Ic}}(\alpha,\beta)$	normalized anisotropy function of K_{Ic} or σ_{Ic} as a function of angles α and β
H	Heaviside step function
K_{I}	mode I stress-intensity factor
K_{Ic}	critical mode I stress-intensity factor
k_{BV}	Batdorf crack density coefficient
$\overline{k}_{BV}$	Batdorf uniaxial stress-state normality constant for the volume-flaw failure mode (also known as the Batdorf normalized crack-density coefficient)
k_{wV}	uniaxial Weibull crack-density coefficient
m_{eV}	Weibull modulus for the volume-flaw failure mode for compressive stress states
m_V	Weibull modulus for the volume-flaw failure mode
n	number of incremental links; number of failure modes
$P(X = x)$	probability that a discrete real-valued random variable X equals a possible value x
P_f	probability of failure ($P_f = 1 - P_s$)
P_{fV}	probability of failure of material volume
ΔP_{fV}	probability of failure of a crack with a strength between σ_{Ic} and $(\sigma_{Ic} + \Delta\sigma_{Ic})$ in ΔV
$(P_{fV})_i$	probability of failure of the i^{th} link
P_s	reliability or probability of survival ($P_s = 1 - P_f$)
P_{sV}	probability of survival of material volume V
$(P_{sV})_i$	probability of survival of the i^{th} link
ΔP_{1V}	probability of existence of a crack with strength between σ_{Ic} and $(\sigma_{Ic} + \Delta\sigma_{Ic})$ in an incremental volume
P_{2V}	probability that a crack of critical strength will be oriented in a particular direction such that it will grow and cause failure
p	success probability

$\wp(\alpha, \beta)$	probability that a crack of critical stress σ_{Ieqc} is oriented in the range between α and $(\alpha + d\alpha)$ and between β and $(\beta + d\beta)$
$\wp_c(\Sigma, \alpha, \beta)$	probability that the critical flaw (the failure-initiating flaw) is oriented in the range between α and $(\alpha + d\alpha)$ and between β and $(\beta + d\beta)$ under stress state Σ
$\wp_\angle(\alpha, \beta)$	probability density distribution (PDD) function of $\wp(\alpha, \beta)$
$\wp_\angle(\Sigma, \alpha, \beta)$	PDD function of the orientation of critical flaw normals from the applied stress state Σ given by angles α and β
r_L	constant (ratio) or parameter in K_{Ic} anisotropy function for polar-cap distribution
r_T	constant (ratio) or parameter in K_{Ic} anisotropy function for equatorial-belt distribution
s	slope of a line
V	volume
ΔV	incremental volume
ΔV_i	incremental volume associated with the i^{th} link
X	discrete real-valued random variable
x	real valued number; possible value of discrete real-valued random variable X
x, y, z	location in the body of the structure; Cartesian coordinates
Y	crack-shape geometry factor
α, β	orientation angles or angular coordinates, where the direction normal to the plane of the microcrack is specified by the radial line defined by α and β in stress space
γ	constant or parameter in K_{Ic} anisotropy function representing the exponent of the sine or cosine function
γ_L	constant or parameter in K_{Ic} anisotropy function representing the longitudinal (polar-cap) distribution
γ_T	constant or parameter in K_{Ic} anisotropy function representing the transverse (equatorial-belt) distribution
$\zeta(\alpha)$	ζ as a function of angle α describing the anisotropy of flaw orientation
$\zeta(\alpha, \beta)$	function describing the anisotropy of the flaw orientation where the normal direction to the flaw plane is given by angles α and β
η_V	crack-density function
$\eta_V(\alpha, \beta)$	crack-density function dependent on angles α and β
$\eta_V(\sigma)$	crack-density function for applied uniaxial stress, where σ is the number of flaws per unit volume with strength equal to or less than σ
$\eta_V(\sigma_{Ieqc})$	crack-density function for equivalent mode I strength, σ_{Ieqc}, of a flaw: number of flaws per unit volume with strength equal to or less than σ_{Ieqc}
θ	angle of crack propagation relative to the initial plane of the microcrack
Λ	constant or parameter in flaw-orientation anisotropy function representing one-half of the total angular extent of the anisotropy distribution

Λ_L	constant or parameter in flaw-orientation anisotropy function representing the longitudinal (polar-cap) distribution
Λ_T	constant or parameter in flaw-orientation anisotropy function or in K_{Ic} anisotropy function representing the transverse (equatorial-belt) distribution
λ	positive number
ν	Poisson's ratio
ξ_L	constant or parameter in K_{Ic} anisotropy function representing the longitudinal (polar-cap) distribution
ξ_T	constant or parameter in K_{Ic} anisotropy function representing the transverse (equatorial-belt) distribution
Σ	summation function; applied far-field multiaxial stress state
σ	applied uniaxial stress
σ_{Ic}	critical mode I strength
$\overline{\sigma}_{Ic,x}$, $\overline{\sigma}_{Ic,y}$, $\overline{\sigma}_{Ic,z}$	orthogonal critical strength components normalized by $\sigma_{Ic,max}$
σ_{Ieq}	equivalent, or effective, stress
$\sigma_{Ieq,max}$	maximum value of σ_{Ieq} over the unit sphere from the applied multiaxial stress Σ
$\sigma_{Ieq}(x, y, z, \alpha, \beta)$	equivalent, or effective, stress as a function of location x, y, z and orientation α, β
σ_{Ieqc}	critical equivalent, or effective, stress
$\sigma_{Ieqc}(x, y, z, \alpha, \beta)$	mode I far-field strength of a flaw located at coordinates x, y, and z and oriented at angles α and β
σ_i	local uniaxial stress
σ_n	applied far-field stress component normal to a crack face
σ_o	Weibull scale parameter
$\sigma_{o\not{e}V}$	Weibull scale parameter for compression for the volume-flaw failure mode normalized to unit volume
σ_{oV}	Weibull scale parameter for the volume-flaw failure mode normalized to unit volume
σ_{uV}	threshold stress parameter
σ_x, σ_y, σ_z	orthogonal stress components expressed relative to a global coordinate system
τ	shear stress acting on the oblique plane whose normal is determined by angles α and β, which represents the applied far-field shear stress on a crack face
τ_{xy}, τ_{yz}, τ_{zx}	shear stress components expressed relative to a global coordinate system
ϕ	constant or parameter in flaw-orientation anisotropy function representing the exponent of the sine or cosine function
ϕ_L	constant or parameter in flaw-orientation anisotropy function representing the longitudinal (polar-cap) distribution

ϕ_T	constant or parameter in flaw-orientation anisotropy function representing the transverse (equatorial-belt) distribution
$\Omega(\Sigma, \sigma_{Ieqc})$	area of a solid angle projected onto a unit radius sphere in three-dimensional stress space for which $\sigma_{Ieq} \geq \sigma_{Ieqc}$ from an applied multiaxial stress state Σ

Superscript

-	normalized

Subscripts

I, II, III	mode I, II, or III
i	i^{th} value or i^{th} term
L	longitudinal
max	maximum
n	integer; number of links; normal
T	transverse
V	volume or a volume-based property (e.g., indicates volume-flaw analysis)

Definitions

L	longitudinal
mode I	crack-opening mode
mode II	crack-sliding mode (in-plane shear)
mode III	crack-tearing mode (out-of-plane shear)
T	transverse

References

Aboudi, Jacob (1995): Micromechanical Analysis of Thermo-Inelastic Multiphase Short-Fiber Composites. Compos. Eng., vol. 5, no. 7, pp. 839–850.

Aboudi, Jacob; Pindera, Marek-Jerzy; and Arnold, Steven M. (2003): Higher-Order Theory for Periodic Multiphase Materials With Inelastic Phases. Int. J. Plast., vol. 19, pp. 805–847.

Batdorf, S.B. (1973): A Statistical Theory for the Fracture of Transversely Isotropic Brittle Materials of Moderate Anisotropy. Air Force Report SAMSO–TR–73–361, Aerospace Report TR–0074 (4450–76)–1, NTIS AD–770982.

Batdorf, S.B. (1978a): Fracture Statistics of Polyaxial Stress States. Fracture Mechanics, Nicholas Perrone, et al., eds., University Press of Virginia, Charlottesville, VA, pp. 579–591.

Batdorf, S.B. (1978b): New Light on Weibull Theory. Nucl. Eng. Des., vol. 47, pp. 267–272.

Batdorf, S.B.; and Crose, J.G. (1974): A Statistical Theory for the Fracture of Brittle Structures Subjected to Nonuniform Polyaxial Stresses. J. Appl. Mech., vol. 41, no. 2, pp. 459–464.

Batdorf, S.B.; and Heinisch, H.L., Jr. (1978): Weakest Link Theory Reformulated for Arbitrary Fracture Criterion. J. Am. Ceram. Soc., vol. 61, nos. 7–8, pp. 355–358.

Bednarcyk, Brett A.; and Arnold, Steven M. (2002): MAC/GMC 4.0 User's Manual—Keywords Manual. NASA/TM—212077/VOL2. http://ntrs.nasa.gov/

Buch, J.D.; Crose, J.G.; and Robinson, E.Y. (1977): Failure Criteria in Graphite Program. AFML–TR–77–16. Available from the Air Force Material Laboratory.

Cady, Carl; Heredia, Fernando E.; and Evans, Anthony G. (1995): In-Plane Mechanical Properties of Several Ceramic-Matrix Composites. J. Am. Ceram. Soc., vol. 78, no. 8, pp. 2065–2078.

Erdogan, F.; and Sih, G.C. (1963): On the Crack Extension in Plates Under Plane Loading and Transverse Shear. J. Basic Eng., vols. 85–86, pp. 519–525.

Evans, A.G. (1978): A General Approach for the Statistical Analysis of Multiaxial Fracture. J. Amer. Ceram. Soc., vol. 61, nos. 7–8, pp. 302–308.

Hellen, T.K.; and Blackburn, W.S. (1975): The Calculation of Stress Intensity Factors for Combined Tensile and Shear Loading. Int. J. Fract., vol. 11, no. 4, pp. 605–617.

Hoel, Paul G.; Port, Sydney C.; and Stone, C.J. (1971): Introduction to Probability Theory. Houghton Mifflin, Boston, MA, pp. 65 and 131.

Ichikawa, M. (1991): Proposal of an Approximate Analytical Expression of Maximum Energy Release Rate of a Mixed Mode Crack in Relation to Reliability Evaluation of Ceramic Components. J. Soc. Mat. Sci. Jpn., vol. 40, pp. 224–227.

Lutz, G. (2006): The Puck Theory of Failure in Laminates in the Context of the New Guideline VDI2014 Part 3. Conference on Damage in Composite Materials 2006, Stuttgart, Germany.

Lynch, Christopher S.; and Evans, Anthony G. (1996): Effects of Off-Axis Loading on the Tensile Behavior of a Ceramic-Matrix Composite. J. Am. Ceram. Soc., vol. 79, no. 12, pp. 3113–3123.

Matsuo, Yotaro (1981): A Probabilistic Analysis of the Brittle Fracture Loci Under Bi-Axial Stress State: 1st Report; In the Case of Tension Being Dominant. Bull. JSME, vol. 24, no. 188, pp. 290–294.

Nemeth, Noel N. (2013): Unit-Sphere Multiaxial Stochastic-Strength Model Applied to Anisotropic and Composite Materials. NASA/TP—2013-217749, 2013. http://ntrs.nasa.gov/

Nemeth, Noel N.; and Bratton, Robert L. (2011): Statistical Models of Fracture Relevant to Nuclear-Grade Graphite: Review and Recommendations. NASA/TM—2011-215805. http://ntrs.nasa.gov/

Nemeth, Noel N., et al. (2003): CARES/Life Ceramics Analysis and Reliability Evaluation of Structures Life Prediction Program. NASA/TM—2003-106316. http://ntrs.nasa.gov/

Nemeth, Noel N.; Gyekenyesi, J.P.; and Jadaan, Osama M. (2005): Lifetime Reliability Prediction of Ceramic Structures Under Transient Thermomechanical Loads. NASA/TP—2005-212505. http://ntrs.nasa.gov/

Nemeth, Noel N.; Manderscheid, Jane M.; and Gyekenyesi, John P. (1990): Ceramics Analysis and Reliability Evaluation of Structures (CARES). Users and Programmers Manual. NASA TP–2916. http://ntrs.nasa.gov/

Shetty, D.K. (1987): Mixed-Mode Fracture Criteria for Reliability Analysis and Design With Structural Ceramics. J. Eng. Gas Turbines Power, vol. 109, no. 3, pp. 282–289.
Weibull, Waloddi (1939): A Statistical Theory of the Strength of Materials. Ingeniorsvetenskapsakademiens Handlingar, no. 151.

REPORT DOCUMENTATION PAGE	Form Approved OMB No. 0704-0188

1. REPORT DATE *(DD-MM-YYYY)*	2. REPORT TYPE	3. DATES COVERED *(From - To)*
01-09-2013	Technical Memorandum	

4. TITLE AND SUBTITLE
Unit-Sphere Anisotropic Multiaxial Stochastic-Strength Model Probability Density Distribution for the Orientation of Critical Flaws

5a. CONTRACT NUMBER

5b. GRANT NUMBER

5c. PROGRAM ELEMENT NUMBER

6. AUTHOR(S)
Nemeth, Noel, N.

5d. PROJECT NUMBER

5e. TASK NUMBER

5f. WORK UNIT NUMBER
WBS 984754.02.07.03.16.03.02

7. PERFORMING ORGANIZATION NAME(S) AND ADDRESS(ES)
National Aeronautics and Space Administration
John H. Glenn Research Center at Lewis Field
Cleveland, Ohio 44135-3191

8. PERFORMING ORGANIZATION REPORT NUMBER
E-18546-2

9. SPONSORING/MONITORING AGENCY NAME(S) AND ADDRESS(ES)
National Aeronautics and Space Administration
Washington, DC 20546-0001

10. SPONSORING/MONITOR'S ACRONYM(S)
NASA

11. SPONSORING/MONITORING REPORT NUMBER
NASA/TM-2013-217810

12. DISTRIBUTION/AVAILABILITY STATEMENT
Unclassified-Unlimited
Subject Category: 37
Available electronically at http://www.sti.nasa.gov
This publication is available from the NASA Center for AeroSpace Information, 443-757-5802

13. SUPPLEMENTARY NOTES
An Erratum was added to this report March 2014.

14. ABSTRACT
Models that predict the failure probability of monolithic glass and ceramic components under multiaxial loading have been developed by authors such as Batdorf, Evans, and Matsuo. These “unit-sphere” failure models assume that the strength-controlling flaws are randomly oriented, noninteracting planar microcracks of specified geometry but of variable size. This report develops a formulation to describe the probability density distribution of the orientation of critical strength-controlling flaws that results from an applied load. This distribution is a function of the multiaxial stress state, the shear sensitivity of the flaws, the Weibull modulus, and the strength anisotropy. Examples are provided showing the predicted response on the unit sphere for various stress states for isotropic and transversely isotropic (anisotropic) materials--including the most probable orientation of critical flaws for offset uniaxial loads with strength anisotropy. The author anticipates that this information could be used to determine anisotropic stiffness degradation or anisotropic damage evolution for individual brittle (or quasi-brittle) composite material constituents within finite element or micromechanics-based software.

15. SUBJECT TERMS
Batdorf; Failure probability; Multiaxial; Strength; Probability density function; Flaw orientation; Unit sphere; Anisotropy; Transverse isotropy

16. SECURITY CLASSIFICATION OF:			17. LIMITATION OF ABSTRACT	18. NUMBER OF PAGES	19a. NAME OF RESPONSIBLE PERSON
a. REPORT	b. ABSTRACT	c. THIS PAGE			STI Help Desk (email:help@sti.nasa.gov)
U	U	U	UU	46	19b. TELEPHONE NUMBER *(include area code)* 443-757-5802